IVYSPRING INTERNATIONAL PUBLISHER

Theranostics

2026; 16(14): 7869-7896. doi: 10.7150/thno.132719

Review

Recent advances in targeting cyanine dyes: hierarchical targeting mechanisms and theranostic integration for multi-disease precision therapy

Shuai Zhang, Yang Xu, Yu Wang, Zelin Chen, Yang Wang, Quanying Liu, Tantan Wang, Yali Dai, Chunmeng Shi✉

Institute of Rocket Force Medicine, State Key Laboratory of Trauma and Chemical Poisoning, College of Preventive Medicine, Army Medical University (Third Military Medical University), Chongqing 400038, China.

✉ Corresponding author: E-mail: shicm@tmmu.edu.cn.

Received: 2026.02.05; Accepted: 2026.05.31; Published: 2026.06.25

Abstract

The development of novel theranostic agents is a key initiative to address current limitations in disease diagnosis and therapy. Notably, targeting cyanine dyes (TCDs), by virtue of their excellent optical imaging performance, versatile structural modifiability, and multi-dimensional targeting specificity, facilitate the directional recognition of disease regions and exhibit tremendous application potential in theranostics. While a variety of TCDs have been successfully developed and their theranostic efficacy experimentally validated, researchers still lack a systematic summary of related studies. Although related advances in fluorescent probes, tumor theranostics, and NIR-II fluorophores have been reviewed, a focused and systematic overview of TCDs in terms of their synthesis, hierarchical targeting mechanisms, and multi-disease theranostic applications remains limited. Accordingly, this article systematically reviews TCDs' synthesis strategies, elucidates their "tissue-cell-organelle" hierarchical targeting mechanism, and summarizes the therapeutic applications in diseases including tumors, fibrotic diseases, metabolic diseases, and radiation-induced injuries. Compared with previous reviews, this review highlights the structure-inherent targeting properties of TCDs, their hierarchical targeting mechanisms, and their emerging theranostic potential beyond oncology. Meanwhile, this article outlines the core advantages and current challenges of TCDs in theranostic integration, and delineates key future directions, including precise and intelligent molecular design, photostability limitations, systematic preclinical evaluation, multimodal technology integration, and the expansion of disease application scenarios. It aims to provide comprehensive theoretical support for advancing the fundamental research and clinical translation of TCDs.

Keywords: near-infrared fluorescence imaging, targeting cyanine dyes, heptamethine cyanine dyes, theranostic integration, precision disease therapy

1. Introduction

Conventional diagnostic and therapeutic approaches have many limitations in practical application [1, 2], including insufficient specificity [3-5], unsatisfactory therapeutic effects [6], and prominent adverse reactions [7, 8]. Accordingly, improving the overall efficiency of disease detection and treatment remains a major challenge in biomedicine. Therefore, developing novel diagnostic and therapeutic tools with high targeting ability and multi-modal functionality has become the key to overcoming the current challenges in diagnosis and treatment [9].

Cyanine dyes, as a class of small-molecule compounds with unique optical and chemical properties, offer a novel technical approach to addressing the aforementioned theranostic challenges. Cyanine dyes include multiple subtypes, with heptamethine cyanine dye and hemicyanine dye being the two mainstream categories. Their core structure consists of two heterocyclic rings connected by a π-conjugated polymethine chain, and the diverse combinations of heterocyclic ring types and side-chain substituents provide ample opportunities to regulate optical properties [10-13]. These dyes typically exhibit near-infrared (NIR) absorption and emission wavelengths (700-1000 nm), allowing effective tissue

penetration, reduced autofluorescence interference, and high sensitivity for *in vivo* imaging [14]. Traditionally, cyanine dyes (such as indocyanine green, ICG) have been recognized as non-targeting agents. Since 2008, our group and collaborators first reported the preferential accumulation of IR-780 dye and its derivatives in malignant tissues through an intrinsic targeting mechanism without any structural modification, targeting ligand, or nanocarrier, providing a structure-inherent active targeting modality for medical imaging and theranostics [15]. This unexpected finding suggested a top-down strategy and upended the prevailing bottom-up strategy that selective drug delivery requires molecular complexity, and was subsequently validated by independent laboratories worldwide. To clearly define such targeting functional materials, this review refers to cyanine dyes with actively structure-inherent targeting recognition capabilities as targeting cyanine dyes (TCDs).

The multi-dimensional targeting capabilities of TCDs exhibit distinct hierarchical characteristics, which can achieve precise targeting recognition at the tissue, cell, and subcellular levels [16-18]. Specifically, this targeting function can be achieved through different pathways: regulating the hydrophilicity/hydrophobicity, charge state of molecules, or utilizing inherent pathological microenvironment features such as hypoxia and high glycolysis, and each level of targeting is closely associated with theranostic applications. At the tissue, TCDs accumulate in pathological sites stress and energy-dependent via the enhanced permeability and retention (EPR) effect or specific ligand-receptor interactions [19, 20]. Moving to the cellular, transmembrane transport mediated by organic anion transporting polypeptides (OATPs) and albumin-receptor-mediated endocytosis enables TCDs to accurately recognize multiple specific pathology-related cells [21, 22]. At the organelle level, these dyes may preferentially localize to mitochondria via lipophilic cationic properties, energy-dependent, and transporter-mediated pathways [23, 24], directly regulating cellular energy metabolism and apoptotic pathways [25, 26]. We propose this multi-dimensional targeting as a stress-induced selective enrichment (SISE) mechanism, allowing TCDs to serve as precise fluorescent imaging probes and agents for photothermal therapy (PTT), photodynamic therapy (PDT), or the regulation of pathological pathways, thereby constructing a novel "theranostics integration" model [27]. Currently, TCDs have achieved significant advances in both fundamental research and application across a range of diseases, including tumor, fibrotic diseases, metabolic disorders, and radiation-induced injuries (RII). For example, IR-34 can also target mitochondrial protein NDUFS1 while completing imaging in cancer cells, significantly inhibiting tumor growth and recurrence [28]. Notably, IR-780 identifies glycolytic fibroblasts, and when combined with PTT and PDT, enhances its cytotoxicity towards these cells, providing a potential technique for targeted intervention in fibrotic diseases [27]. In addition, TCDs can also exhibit good preventive effects on chronic diseases. For instance, IR-61 can accumulate in the mitochondria of macrophages in adipose tissue, inhibiting macrophage activation and effectively preventing chronic inflammation, weight gain, and metabolic disorders [29]. IR-61 can also exert a protective effect on radiation-induced lung injury (RILI). Specifically, it targets the mitochondria of macrophages within irradiated lung tissue, upregulating *Nrf2* and heme oxygenase-1 (HO-1), reducing reactive oxygen species (ROS) and pro-inflammatory factors (IL-1β, IL-6), and alleviating radiation-induced lung tissue damage [30].

Despite significant progress in TCD-based disease theranostics, several limitations remain: for instance, IR-780 has strong hydrophobicity and may pose potential safety risks due to poor biocompatibility [22]; ZWZ-3 only conducted cell/animal efficacy tests, and the *in vivo* metabolic process is still unclear [31]; the most important point is that currently most dyes are still in basic research without any clinical trial data, lacking systematic exploration from basic research to clinical applications. Our group has pursued sustained research in this field for many years and has made significant advances in the precise theranostics of various diseases, including tumors, fibrotic diseases, metabolic disorders, and RII. Based on a profound understanding of the field's current status and development potential, this review (**Figure 1**) systematically summarizes TCDs' synthesis strategies, targeting mechanism classifications, multi-disease theranostic application progress, and core molecular mechanisms, while proposing key future research directions addressing current challenges. Ultimately, this review aims to provide a comprehensive research perspective, engage more interdisciplinary researchers, and facilitate the advancement of basic research on TCDs and their clinical translation.

2. Synthesis Strategies of TCDs

With outstanding optical performance and flexible structural modification space, TCDs have risen to become outstanding NIR fluorescent dyes [32-36]. Its excitation wavelength matches the biological NIR optical window, offering outstanding tissue penetration capabilities. Leveraging their wavelength

advantages and excellent biocompatibility, heptamethine cyanine dyes and hemicyanine dyes are widely used in bioimaging and phototherapy. The following sections will introduce their synthetic routes and review the latest advancements in functional modifications.

2.1 Synthesis of Heptamethine Cyanine Dyes

Heptamethine cyanine dyes (Cy7) are composed of a heptamethine bridge connecting nitrogen-containing heterocyclic chromophores such as indole and benzindole. Their conjugated structure confers NIR optical properties, while the terminal rings, N-substituents, inner positions, and side chains can all undergo structural modifications. Based on molecular symmetry, they can be classified into symmetric and asymmetric types, which exhibit distinct synthetic approaches and functional characteristics [37].

The highly symmetrical planar configuration facilitates π-electron delocalization in symmetric heptamethine cyanine dyes, enabling tunable high-performance NIR absorption and fluorescence in the 700-900 nm wavelength range [38]. This type of dye has a high molar extinction coefficient, efficiently capturing light and exhibiting excellent light absorption properties [39]. Moreover, strategic structural modifications, notably meso-substitution, serve as a powerful lever to fine-tune their performance [40]. Recent work indicates that scaffold tuning can push symmetric heptamethine cyanine dyes into the NIR-II region, supporting their use in deep-tissue imaging and spectral extension [41]. Symmetric heptamethine cyanine dyes tend to have balanced electronic structures and predictable photophysical behavior. Asymmetric analogues, however, introduce electronic and steric imbalance through different terminal heterocycles or uneven polymethine substituents, making them easier to tune for solubility, charge distribution, targeting, and stimulus response. Therefore, both symmetric and asymmetric derivatives have been extensively developed as important structural platforms for functional heptamethine cyanine dyes, and representative examples are summarized in **Figure 2**.

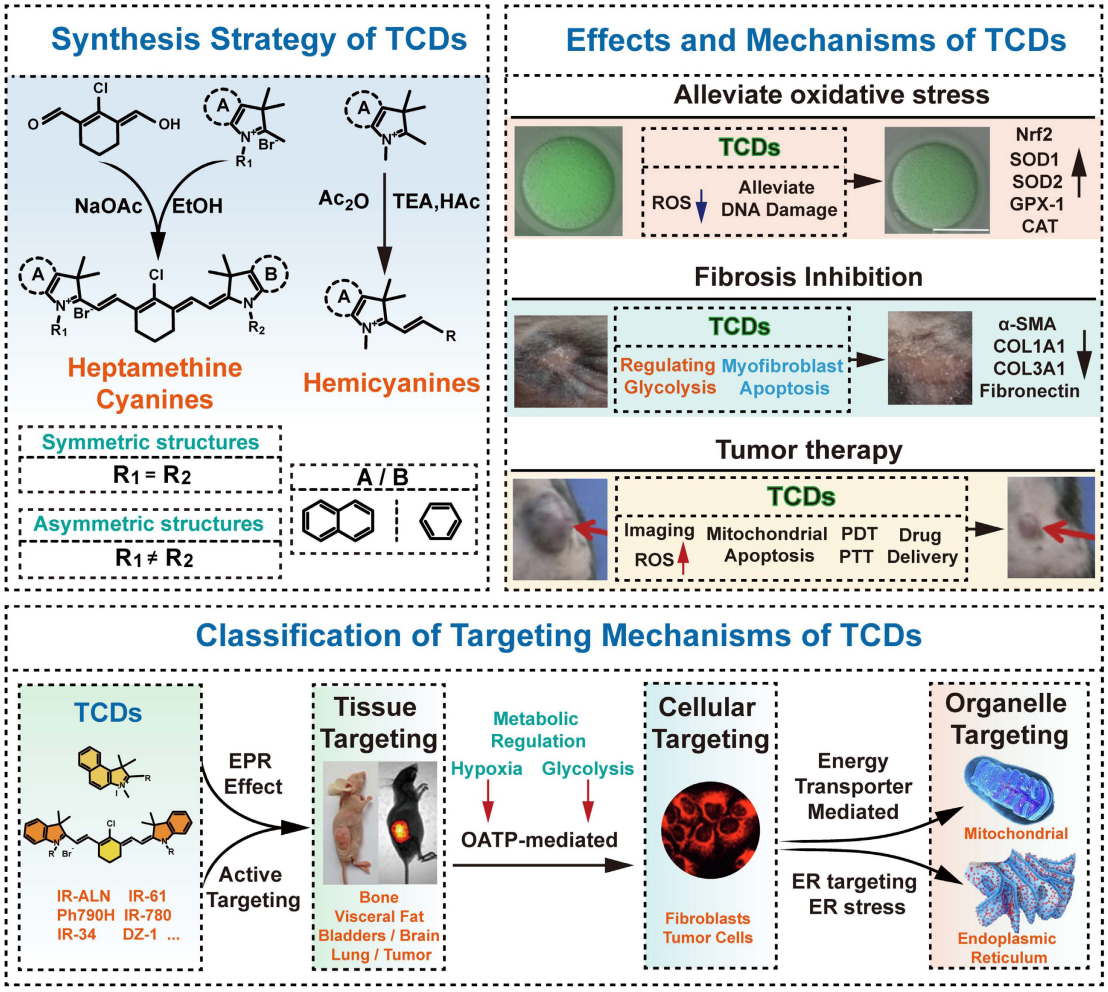

Figure 1. Schematic diagram demonstrate TCD synthesis strategies in this review, alongside an analysis of their hierarchical targeting mechanisms and therapeutic applications for various diseases.

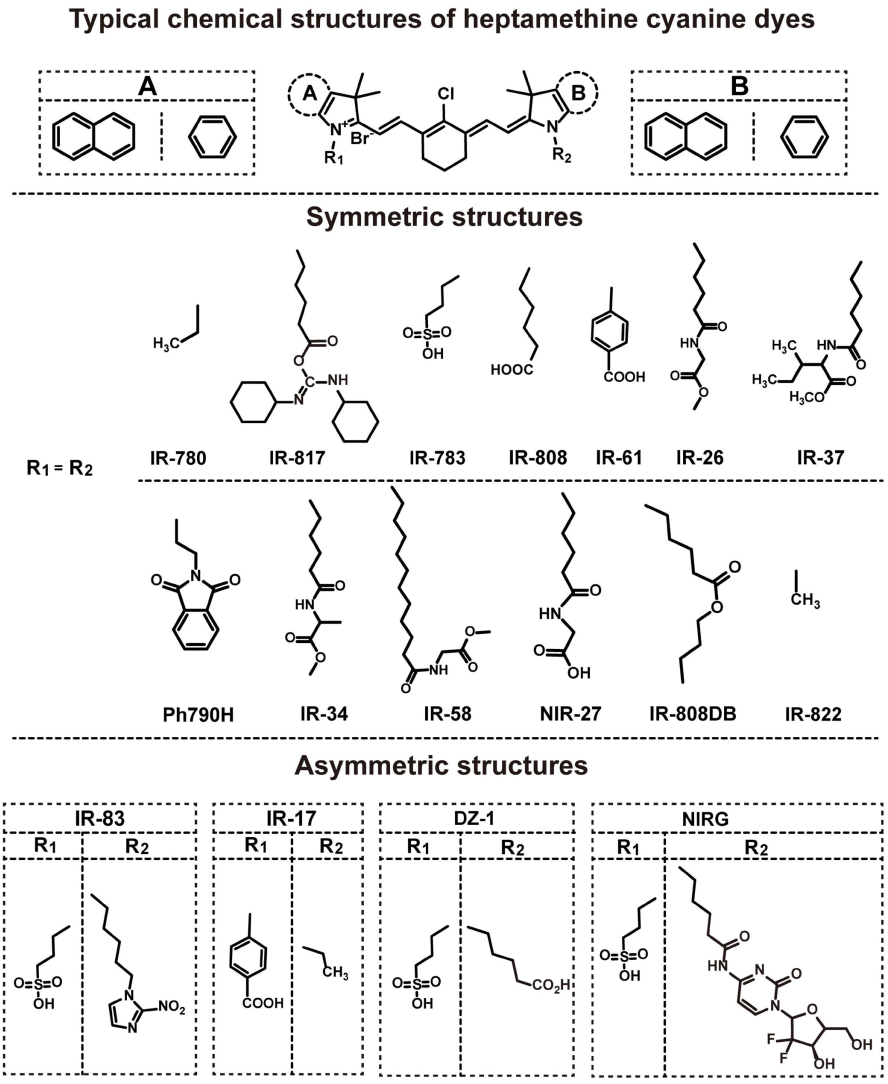

Figure 2. Schematic representation of the typical core structure of heptamethine cyanine dyes and summary of their structural classification. By varying the substituents (R_1 and R_2) and terminal groups, a wide range of derivatives has been developed. These compounds are broadly divided into symmetric ($R_1 = R_2$) and asymmetric ($R_1 \neq R_2$) types, with representative examples shown for each category.

Based on these advantages, most of the TCDs in current research are symmetrical heptamethine cyanine dyes, and the synthesis scheme of these dyes can be summarized as follows (**Figure 3A**): Firstly, the synthesis of the meso-chlorocyclohexenecarbaldehyde intermediate (**2b**): Cyclohexanone (**2a**) reacts with a mixture of dimethylformamide (DMF) and phosphorus oxychloride ($POCl_3$) at room temperature for 5 h, then washed with water and recrystallized from dichloromethane to afford 2-chloro-1-formyl-3-(hydroxymethylene) cyclohex-1-ene (**2b**) [42]. Secondly, the synthesis of indole quaternary ammonium salts (**2e**): Phenylhydrazine (**2c**) reacts with 3-methyl-2-butanone under acidic conditions (AcOH) through a one-pot method to generate 2,3,3-trimethyl-3H-indole (**2d**) [43]. Subsequently, **2d** reacts with brominated compounds in 1,2-dichlorobenzene at 110 °C for 10 h to yield N-alkylated indole quaternary ammonium salts (**2e**) [44, 45]. Thirdly, condensation to form the target dye (**2f**): **2b** and **2e** are refluxed together at 80 °C for several hours in anhydrous ethanol containing anhydrous sodium acetate, affording a series of symmetric heptamethine cyanine dyes (**Figure 2**). The syntheses of Ph790H and CA800Cl differ mainly in the final construction of the cyanine scaffold. For Ph790H, the concluding step employs N-[(3-(benzylidene)-2-chloro-1-cyclohexen-1-yl)methylene]aniline hydrochloride (**2g**) rather than **2b**, reacting **2g** with **2e** in an ethanol/sodium acetate system under reflux for 6 hours to afford the target molecule [46]. CA800Cl is prepared through a different route: 4-hydrazidobenzoic acid (**2h**) reacts with 3-methyl-2-butanone in glacial acetic acid to form carboxylated indole (**2i**), followed by heterocyclic salt (**2j**) and final conversion to CA800Cl [47].

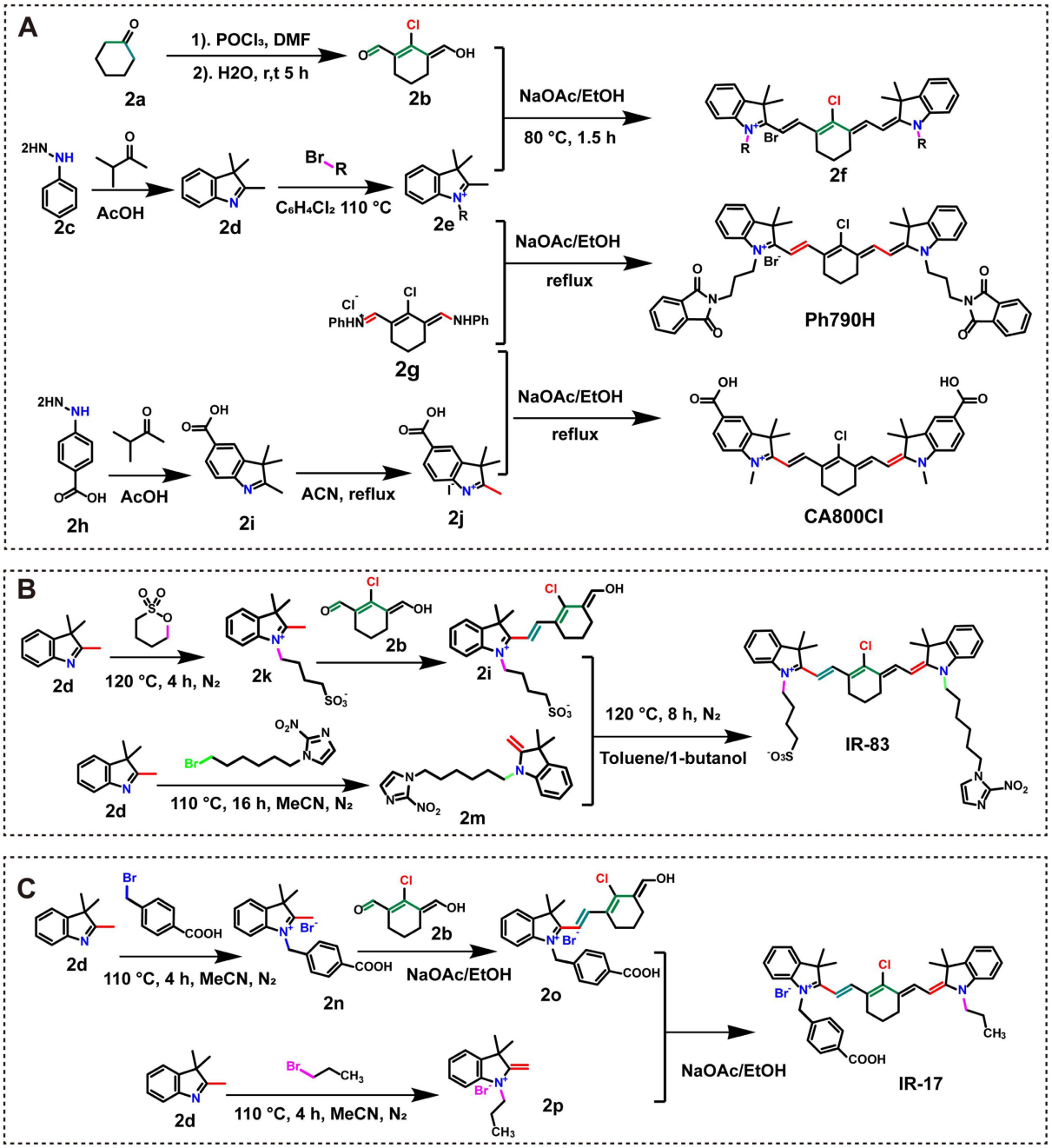

Figure 3. Synthetic routes for heptamethine cyanine dyes. (A) Preparation of symmetric heptamethine cyanine dyes. (B-C) Construction of asymmetric heptamethine cyanine dyes.

Despite the dominance of symmetric heptamethine cyanine dyes, asymmetric analogues are increasingly useful for imaging and therapy because they combine larger Stokes shifts, disease-responsive activation, and improved organelle targeting or tumor retention [48-51]. They are typically synthesized through stepwise coupling of two distinct indolium salts. In the synthesis of IR-83 (**Figure 3B**): First, 2,3,3-trimethyl-3H-indole (**2d**) reacts with 1,4-butanesultone at 120 °C for 4 h under a nitrogen atmosphere. This yields 2,3,3-trimethyl-1-(4-sulfobutyl)-3H-indolium (**2k**), which then reacts with **2b** to form **2l**. Second, **2d** reacts with 1-(6-bromohexyl)-2-nitro-1H-imidazole to afford **2m**. Finally, **2l** and **2m** are refluxed at 120 °C for 8 h in a toluene/1-butanol system under nitrogen protection. IR-83 is obtained after purification [52]. **Figure 3C** depicts a comparable strategy employed for the synthesis of IR-17. In this case, the key step is the stepwise addition of two distinct functional moieties, leading to the successful assembly of the asymmetric heptamethine cyanine dye [48].

2.2 Modification of Heptamethine Cyanine Dyes

In recent studies, the performance of heptamethine cyanine dyes has often been improved through rational structural modification. By coupling different functional groups, researchers can tune their optical properties, enhance their targeting behavior, and introduce therapeutic functions. These strategies mainly include backbone modification, targeting-motif introduction, and therapeutic-agent conjugation.

(1) Coupling of therapeutically active moieties: As shown in **Figure 4A**, Sun *et al.* synthesized IR-817 by reacting IR-808 with dicyclohexylcarbodiimide in DMF at room temperature, followed by imine-bond condensation with carboxyl groups. The resulting dye preferentially localized in cancer-cell mitochondria and selectively inhibited melanoma cells [18]. Our group modified the N-alkyl chain of IR-808 and subjected the modified intermediate to reaction in a toluene-n-butanol system for 10-20 h to yield IR-DBI. This compound not only exhibits NIR emission capability but also targets cancer cell mitochondria and selectively suppresses melanoma [53]. Its asymmetric amphiphilic structure facilitates cell membrane translocation and mitochondrial targeting, while self-assembles with albumin into complexes to enhance tumor accumulation via the EPR effect [54, 55].

(2) Targeting ligand modification: Based on the significant affinity of bisphosphonates (such as alendronate sodium, ALN) toward hydroxyapatite [16], our research group designed and synthesized a bone-targeted dye IR783-ALN. The specific synthesis route is shown in **Figure 4B.** Firstly, IR-783 was used as a precursor and reacted with 3-mercaptopropionic acid in DMF solvent with stirring at 40 ℃ for 18 h to obtain the intermediate IR-783-3Q; subsequently, the intermediate was placed in a sodium borate buffer system and coupled with ALN to obtain the bone-targeted dye IR783-ALN [56]. In addition, in response to the demand for tumor targeting, researchers prepared another derivative of IR-783, DZ-1, using an ethanol/sodium acetate system through reflux technology. Experimental results have shown that DZ-1 not only improves its hydrophilicity, but also has excellent tumor targeting ability. It can be preferentially taken up by hepatocellular carcinoma cells (HCC) and specifically enriched in the subcellular structures of mitochondria and lysosomes [51, 57, 58].

(3) Theranostic integration modification: Jason Boyang Wu *et al*. conjugated DZ-1 with gemcitabine via an EDC-HOBt activation system for 15 h to yield NIRG (**Figure 4B**), a conjugate that markedly enhances the drug's permeability across the blood-brain barrier (BBB)/blood-tumor barrier (BTB) and prolongs the survival of tumor-bearing mice [59]. Similarly, Meng *et al*. fabricated the smart probe IR822-PY (**Figure 4C**) by stirring the pH-responsive receptor PY with IR-822 in triethylamine at 40 °C for 5 h under nitrogen. This probe integrates dual functions of pH-sensitive imaging and PTT [60]. In another approach, Zhao *et al*. reacted IR-780 with tetraphenylethylene (TPE) in a triethylamine-DMF system at 85 °C for 4 h to yield T780T (**Figure 4D**). The twisted conformation of TPE elevates the photothermal conversion efficiency (PCE) to 38.5% through intramolecular motion in the excited state [61]. Furthermore, Shen *et al*. introduced triphenylphosphine (a mitochondrial targeting moiety) at the meso-position of heptamethine cyanine dyes [62-64], with the reaction proceeding in a triethylamine/DMF system at 70 °C for 2 h to afford Cy750M-C1 (**Figure 4E**). Building on this, subsequent co-assembly with DSPE-PEG_{2000} and DSPE-PEG_{2000}-FA yielded Cy750M-C1-FA-NPs, which achieved remarkable improvements in water solubility, tumor targeting specificity, and intratumoral accumulation [65].

Compared with the above cases, stimuli-responsive activation provides an important pathway for the intelligent design of TCDs [66]. A typical example is the pH-responsive amino heptamethine cyanine dyes probe I_2-IR783-Mpip, in which acid triggered fluorescence recovery is achieved by modifying the median position with N-methylpiperazine, and singlet oxygen generation is enhanced by protonated PET inhibition. The probe exhibits a wide NIR absorption range of 820-950 nm under acidic conditions and can mediate PDT under irradiation at approximately 850 nm [67]. In addition, higher specificity can be achieved through a dual locking strategy, such as the semi cyanine-based nanoprobe DL-P, which can simultaneously respond to lysosomal acidic pH and protease B, thereby releasing $CyNH_2$, activating NIR fluorescence, and activating therapeutic functions [68]. Enzyme activated cyanine probes also provide useful examples for intelligent TCD design. For example, QcyP is a switch type NIR probe based on heptamethine cyanine, which uses phosphate monoesters as alkaline phosphatase (ALP) response units. ALP mediated dephosphorylation triggers rearrangement of the conjugated π-electron system and activates NIR fluorescence, enabling imaging of endogenous ALP in cells and HepG2 tumor-bearing mice [69]. With pH/enzyme-responsive or dual-triggered designs, TCD systems can convert disease-microenvironment cues into linked imaging-therapy outputs, improving specificity while reducing off-target effects.

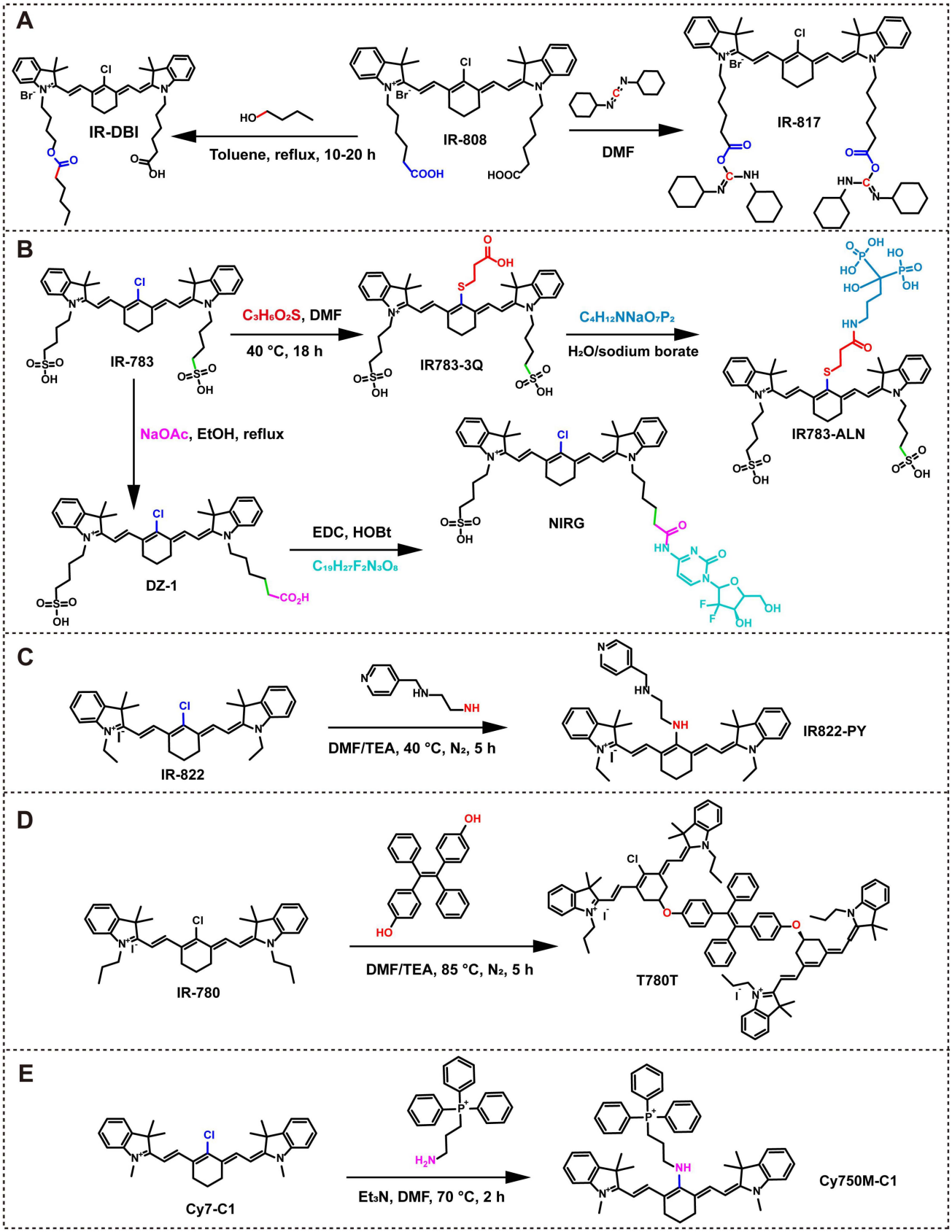

Figure 4. Schematic diagrams of molecular modification for different types of TCDs. (A) Derivatization of IR-808 into IR-DBI and IR-817. (B) Functionalization of IR-783 to yield IR783-ALN and NIRG. (C) Structural modification of IR-822 for the synthesis of IR822-PY. (D) Preparation of T780T based on the IR-780 scaffold. (E) Synthesis of Cy750M-C1 via chemical modification of Cy7-C1.

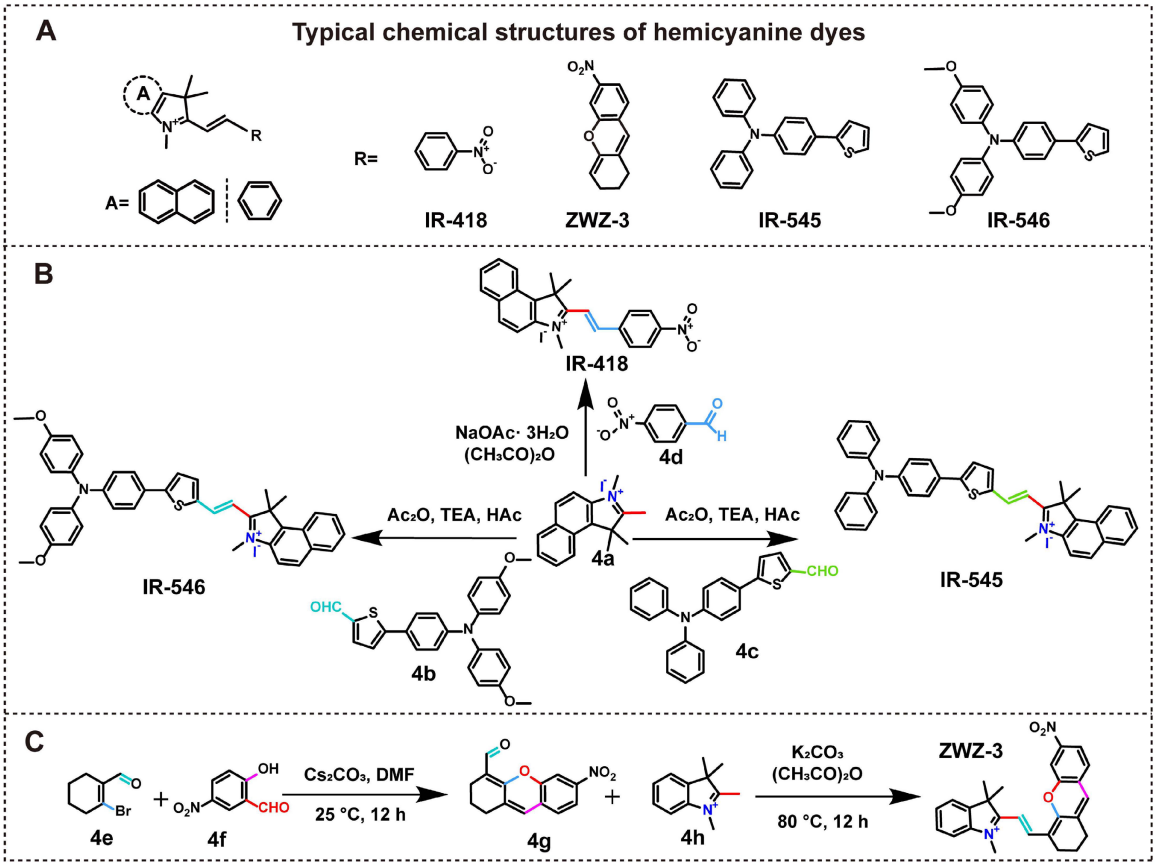

Figure 5. Typical chemical structures and synthetic pathways of representative hemicyanine dyes. (A) Typical chemical structures of hemicyanine dyes. (B) Synthetic pathways leading to IR-418, IR-545, and IR-546 from the precursor 4a. (C) The synthetic route of ZWZ-3 from its starting precursors.

2.3 Synthesis of Hemicyanine Dyes

The unique donor-acceptor (D-A) molecular structure, considerable Stokes shift, and excellent biocompatibility make the hemicyanine dyes a commonly used fluorescent probe for biomedical imaging [70-72]. Its typical structure is the D-π-A configuration (**Figure 5A**), where the conjugated π system bridges the electron donor and the nitrogen-containing heterocyclic acceptor. Thanks to the flexible molecular design, changing the donor unit, acceptor unit, or polyacetylene chain will lead to significant changes in the dye's performance. This type of material synthesis process is simple and straightforward. The core of the process is the condensation reaction between aromatic aldehydes and nitrogen-containing heterocycles to form a conjugated structure. The following text will introduce relevant synthesis examples.

The experiment synthesized IR-546 using 1,2,3,3-tetramethyl-3H-indolium iodide (**4a**) and 5-(4-(bis(4-methoxyphenyl)amino)phenyl)thiophene-2-carbaldehyde (**4b**) as raw materials. The two reactants were first fully dissolved in acetic anhydride, and then triethylamine and acetic acid were added. The reaction was carried out at 60 ℃ with stirring for 1 hour. This route achieved ideal reaction results and the yield of the product was considerable [73]. The synthesis steps of IR-545 are the same as those of IR-546, except that **4b** is replaced by 5-(4-(diphenylamino)phenyl)thiophene-2-carbaldehyde (**4c**) [74]. IR-418 was synthesized using **4a** and 4-nitrobenzaldehyde (**4d**) as raw materials. The reaction was carried out at room temperature in a mixture of sodium acetate trihydrate and acetic anhydride for 1 day. The product is shown in **Figure 5B** [75]. The preparation process of ZWZ-3 differs from the aforementioned single condensation reaction (**Figure 5C**).

Firstly, 2-bromocyclohex-1-ene-1-carbaldehyde (**4e**) and 2-hydroxy-5-nitrobenzaldehyde (**4f**) were fully dissolved in the cesium carbonate modified DMF solvent and stirred at room temperature for 12 hours to complete the preparation of intermediate 6-nitro-2,3-dihydro-1H-xanthene-4-carbaldehyde (**4g**). Subsequently, using **4g** and **4h** as reaction raw materials, relying on the composite system of potassium carbonate and acetic anhydride, a constant temperature reaction was carried out at 80 ℃ for 12 hours, and finally afforded the target dye ZWZ-3 [31].

In summary, the synthetic system of TCDs centers on structural tunability and is guided by functional adaptability, creating a multi-level framework for preparation and modification. By employing symmetrical or asymmetrical molecular synthesis design, researchers can flexibly control the NIR optical properties of heptamethine cyanine dyes. The core regulatory mechanism lies in precisely controlling the π-electron delocalization state and rationally arranging the functional groups on the molecular surface, thereby achieving the targeted optimization of the dye's performance. Researchers are increasingly moving past traditional synthetic routes by employing cyanine dyes as luminescent centers to build structurally defined dendritic nanodots. By progressively assembling polylysine dendritic structures with Cy3/5/7 as the core, fluorescent-tunable, photostable, and biocompatible nanodots can be prepared [76]. The subsequent conjugation of targeting or therapeutic groups demonstrates the advantage of integrated diagnosis and treatment, effectively promoting the clinical translation of TCDs.

2.4 Structure-Activity Relationships of TCDs

Based on clear structure-activity relationships (SARs), TCDs can effectively modulate their optical properties, physicochemical characteristics, and targeting capabilities with only minor structural adjustments. The heptamethine polymethine skeleton is the core of TCDs. Its conjugated methyl unit dominates the basic optical properties of NIR [20, 28, 53, 77]. The extended π system ensures stable NIR fluorescence and enables precise control of the amphiphilic balance. This strategy achieves two benefits in one: it enhances the tissue permeability of short-chain dyes and alleviates the common toxicity and aggregation quenching problems of long-chain alkyl substituents [42,53]. With its lipophilic cationic properties and OATP transport mechanism, this scaffold can penetrate deep into tissues and target accumulation at high metabolic lesions. Further locking the cyclohexene ring in the poly(methyleneimine) bridge to increase structural rigidity not only reduces non-radiative decay but also significantly enhances its selective retention effect at the tumor site [28, 53, 78].

The key to determining the solubility, pharmacokinetics, and subcellular distribution of TCDs lies in peripheral functional modifications rather than the core skeleton. For example, the carboxyl-substituted benzyl-N-alkyl chain of IR-61/817 confers moderate water solubility and achieves mitochondrial targeting through membrane potential driven mechanisms [20, 29]. Sulfonic functionalized derivatives such as DZ-1 and IR-783 exhibit different advantages: they can improve water solubility, accelerate clearance *in vivo*, and do not weaken the original tumor binding ability [78]. Amino acid modification (such as NIR-27 grafted with glycine) can effectively improve biocompatibility [79]. Asymmetric amphiphilic substituents such as IR-DBI enhance the binding affinity of albumin, thereby optimizing pharmacokinetics and promoting tumor targeted delivery through the EPR effect [53].

Based on the advantages of this structure, the derivatization strategy can endow TCDs with new functional characteristics while retaining their inherent targeting properties. Representative approaches include drug conjugation (e.g., 780-5FU and FTS-148), twisted structural design to suppress π-π stacking (e.g., T780T), and carrier-assisted formulations such as BSA@IR-817 and HSA@IR-DBI [20, 53, 78, 80]. The use of this strategy can significantly improve delivery efficiency and effectively suppress fluorescence quenching caused by aggregation. This not only improves the final effect of image-guided therapy, but also perfectly preserves the targeting specificity of the system. The SARs of TCDs are a multidimensional system. The heptamethine skeleton determines the basic optical and targeting properties; side chain modification dominates the physicochemical and biological manifestations; and derivatization further enhances the clinical application value. Based on this structure function association, we were able to deduce the precise targeting mechanism of TCDs, which laid the foundation for the discussion of various treatment strategies in the following text.

3. Classification of Targeting Mechanisms of TCDs

3.1 Tissue Targeting Specificity of TCDs

The prerequisite for achieving precise diagnosis and treatment of TCDs is to overcome the challenge of targeting specificity. By utilizing passive or active targeting mechanisms to promote efficient enrichment of dyes in the lesion area, it can lay the foundation for their subsequent applications.

3.1.1 Passive Targeted Accumulation of TCDs Relying on the EPR effect

Passive targeting utilizes the physiological differences between lesions (such as tumors or inflamed tissues) and healthy tissues to drive dye accumulation [19]. Central to this strategy is the EPR effect. This strategy is based on the EPR effect: the endothelial gap of diseased blood vessels widens (about 100-600 nm) and lymphatic reflux is obstructed, making it easy for molecules or nanoparticles of

appropriate size to penetrate the interstitium and remain [81, 82]. In the TCDs field, this property is utilized to design dyes that bind to serum albumin (BSA/HSA) to construct nanocomplexes [83, 84]. Albumin, as a dual functional carrier, can enhance photostability and inhibit aggregation quenching, while actively promoting tumor enrichment based on the EPR effect [85-87]. Wang *et al*. constructed BSA@IR-817 nanoparticles, enhancing the binding through both covalent and supramolecular interactions. This complex exhibited superior tumor targeting properties compared to the free IR-817, and the fluorescence peaked 6 hours after injection and remained stable for 24 hours [20]. Zhao *et al*. developed T780T nanoparticles, which self-assembled into approximately 200 nm aggregates in water. Utilizing the EPR effect, it achieved sustained tumor enrichment for 96 hours [61]. Furthermore, Tan *et al*. revealed that IR-DBI could bind tightly to site II of HSA and self-assemble into the drug-protein complex HSA@IR-DBI in plasma. Benefiting from the EPR effect, HSA@IR-DBI exhibited higher preferential tumor accumulation in tumor tissues relative to free IR-DBI. Even at 24 h, high-contrast signals between tumors and adjacent marginal regions remained observable (**Figure 6A**) [53]. Additionally, studies have shown that the rigidity of nanoparticles has recently become an important physicochemical parameter for regulating tissue permeability and accumulation. For example, mechanically adjustable dye core polylysine dendrimers exhibit a biological trade-off related to rigidity: Harder nanodots promote deep penetration in 3D tumor spheres, while softer nanodots exhibit longer blood circulation time and enhanced tumor accumulation [88]. The preceding scenario demonstrates that the creation of complexes between TCDs and proteins properly fits the size range of the EPR effect, which can considerably boost the retention effectiveness and longevity of TCDs in tissues. This passive targeting technique effectively addresses the issue of low retention efficiency of free TCDs in tissues. Although the EPR effect has been widely validated in preclinical animal models, its actual efficacy in human tumor treatment remains controversial. The high complexity of human tumors constitutes the main bottleneck. The dense microenvironment, high interstitial hydraulic pressure, and abnormal vascular permeability form multiple physiological barriers. As a result, the *in vivo* accumulation of TCD nanomedicine is extremely unstable, making it difficult to predict whether it is in different tumor types or within a single lesion. This variability greatly reduces the clinical reliability of passive targeted therapy [89]. The inherent heterogeneity of tumors can lead to an uneven spatial distribution of EPR-driven TCDs [90]. Especially in cases where the EPR effect is weak or unstable, a single passive mechanism cannot fully unleash the diagnostic and therapeutic potential of TCDs. Therefore, active targeting must be introduced as a core supplement. This technology not only promotes cellular endocytosis, but also enhances tissue specificity, thereby significantly improving overall therapeutic efficacy.

3.1.2 Active Targeting Mediated by Molecular Modifications

Compared to passively waiting for microenvironmental conditions, active targeting has adopted more proactive intervention measures. Researchers can deliver drugs directly to damaged tissues by adjusting their physicochemical properties or adding targeting groups. This approach eliminates excessive dependence on the EPR effect and ensures delivery reliability even in cases of weak vascular leakage or high tumor heterogeneity. From a molecular mechanism perspective, charge, size, and hydrophobicity determine the permeability and retention ability of dyes [91, 92]; especially lipophilicity plays a central role in promoting dye penetration into adipose tissue [93]. Consider IR-61: because it is both lipophilic and cationic, an intraperitoneal injection allows it to bypass rapid clearance and build up steadily in visceral adipose tissue, aided by the naturally sluggish blood flow in that region [94]. The important approach to achieving active targeting lies in introducing functional groups capable of high-affinity binding to specific tissues into dye molecules via chemical modification. Our group developed IR783-ALN, which mitigates nonspecific protein binding *in vivo* via chlorine-atom substitution on the Cy7 scaffold, while the incorporated bisphosphonate moiety confers targeted bone tissue recognition. After intravenous injection, its fluorescence signal in the distal femur reaches its peak at 24 h and lasts for up to 48 h, indicating strong bone targeting specificity (**Figure 6B**) [56]. This strategy supplemented the poor targeting of free TCDs, and the alteration of particular molecules improves TCDs targeting.

3.2 Cellular Targeting Specificity of TCDs

OATPs are part of the solute carrier organic anion polypeptide transporter family (*SLCO*), which includes six subfamilies (OATP1-OATP6). These transporters can transport many different natural and foreign molecules into cells, providing a basis for TCDs to target specific cells [21].

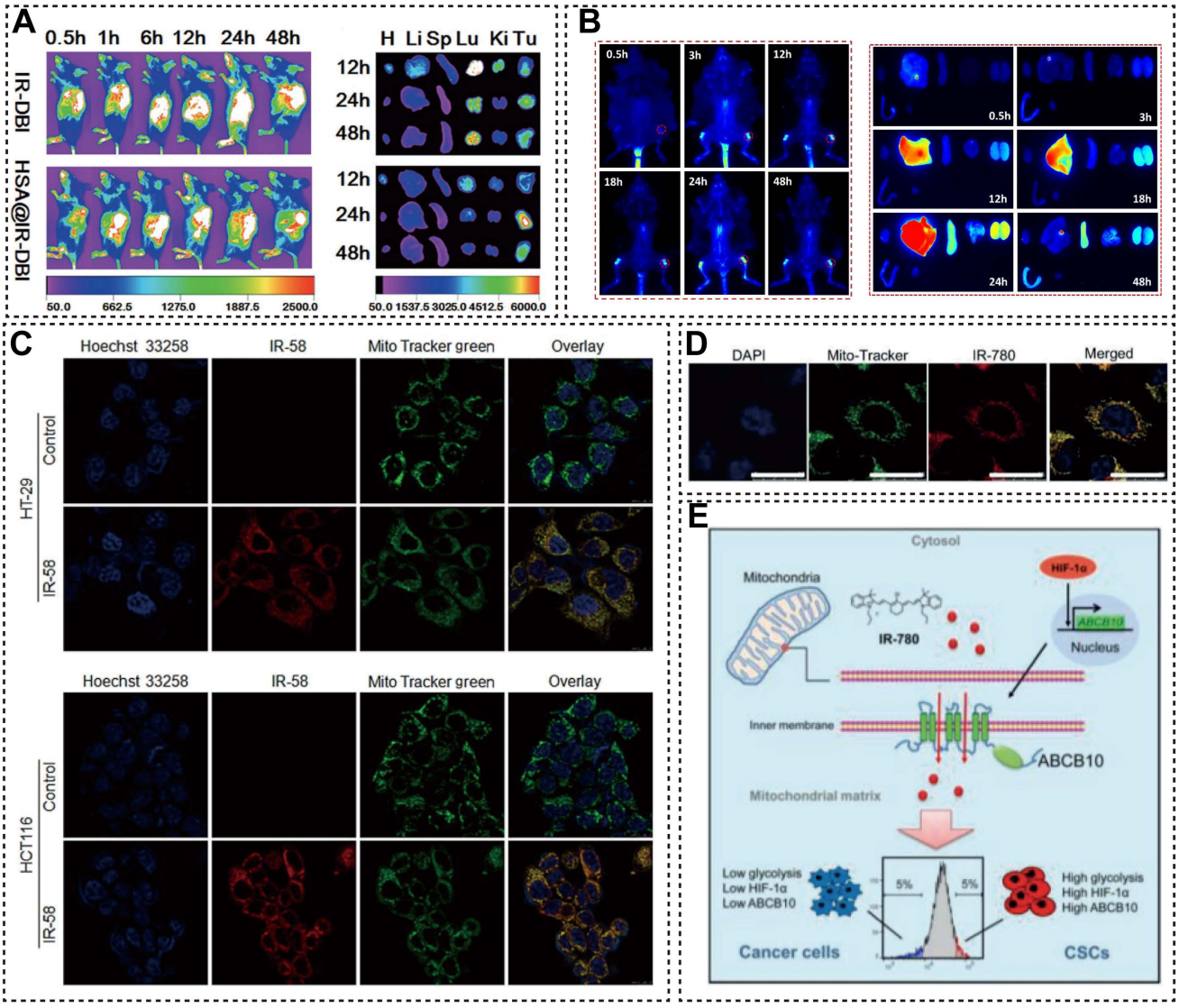

Figure 6. (A) Representative *in vivo* and *in vitro* images of tumor-bearing mice following administration of HSA@IR-DBI and free IR-DBI. Adapted with permission from [53]. Copyright 2017, John Wiley and Sons. (B) NIR fluorescence images of bone tissue and major organs dissected from mice taken at different time points after post-injection of IR-ALN. Adapted with permission from [56]. Copyright 2024, John Wiley and Sons. (C) The co-localization images of IR-58 and mitochondrial-specific tracer in different cells. Adapted with permission from [101]. Copyright 2018, BMJ Publishing Group Ltd. (D) Schematic illustration of HIF-1α/glycolysis-dependent regulation of mitochondrial transporter ABCB10 in characterizing CSCs using IR-780. Adapted with permission from [114]. Copyright 2018, John Wiley and Sons.

3.2.1 OATPs-Mediated Targeted Translocation of TCDs into Fibroblasts

Studies have shown that the specific uptake of TCDs by fibroblasts and their activated subtypes (such as cancer-associated fibroblasts, CAFs) is mainly mediated by specific OATP subtypes, and this process is closely related to cellular glycolytic metabolism [95]. Many research cases have also confirmed this viewpoint. For instance, Meng *et al*. demonstrated that IR-780 can specifically target activated, highly glycolytic fibroblasts via *SLCO2A1*-mediated transmembrane transport, and this preferential accumulation phenotype is regulated by glycolytic metabolism [96]. Wang *et al*. further confirmed that the extensive accumulation of IR-780 in CAFs is associated with high expression of OATP. After intervention with BSP (a competitive OATP inhibitor) and *SLCO2A1* small interfering RNA (siRNA), the uptake of IR-780 by CAFs was significantly reduced, indicating that OATPs (particularly OATP2A1) are the core mediators of specific IR-780 uptake in CAFs [97]. A recent study by Wu *et al*. extended these findings by finding that the entry of IR-780 into fibroblasts depends on the high expression of the OATP1B2 subtype [22]. Chen *et al*. demonstrated that highly active glycolysis and *SLCO2A1* synergistically drive IR-780 uptake in fibroblasts. In fibroblasts cultured under 5% hypoxia, the expression levels of hypoxia-inducible factor-1α (HIF-1α), glycolytic enzymes (LDHA, LDHB, LDHC), and *SLCO2A1* were significantly upregulated; this

effect was reversed by LW6 (a HIF-1α inhibitor), indicating that HIF-1α is a master regulator of the glycolytic phenotype in fibroblasts and *SLCO2A1*-mediated IR-780 uptake [27]. Wang *et al*. discovered that glycolysis enhanced the intracellular retention of IR-780. After using *SLCO4A1* siRNA, the uptake of IR-780 by fibroblasts and myofibroblasts was significantly inhibited [98]. The mechanism of the inhibitory effect of α-KG on HIF-1α is as follows: the HIF-1α/*SLCO4A1* pathway regulates dye internalization, while the active accumulation of the dye is promoted by the *SLCO2A1* transporter through glycolysis activity [99].

3.2.2 OATPs-Mediated Targeted Translocation of TCDs into Tumor Cells

In addition to fibroblasts, OATPs are also a key entry point for various tumor cells to uptake TCD and are closely related to HIF-1α mediated hypoxia signals [100]. Blocking OATPs by BSP can significantly reduce the accumulation of IR-817 in melanoma cells [18], which is also involved in the uptake of IR-58 in HT-29 and HCT116 cells [101]. Further research has shown that the entry of IR-780 into cells depends on energy metabolism, plasma membrane potential, and *OATP1B3*, rather than endocytosis or ABC transporters. It can also avoid the efflux of *ABCB1*/*ABCC1*, thereby maintaining intracellular retention [102]. Hypoxia is closely related to OATP expression. Wu *et al*. found that in prostate cancer, hypoxia can promote HIF-1α binding to the *OATP1B3* promoter and upregulate its transcription, thereby enhancing MHI-148 uptake. Even when *OATP1B3* is knocked down under normoxic conditions, dye uptake still decreases by about 30%, indicating that this process is jointly regulated by hypoxia signaling and OATP expression [99]. The canine model further indicates that HIF-1α stabilization can promote *OATP1B3*/*2B1* expression, while rifampicin and other OATP inhibitors can weaken this effect [103]. Interestingly, OATP activation can also promote drug crossing over the BBB and BTB, and is not entirely dependent on strict hypoxia [59, 104]. Qin *et al*. also confirmed that HIF-1α can bind to the *OATP1B3* promoter HRE sequence to drive transcription, while Abi-DZ-1 enters tumor cells through the HIF-1α/OATP axis [78]. Overall, the tumor targeting of TCDs mainly comes from OATP mediated transport and is jointly influenced by HIF-1α hypoxia signaling and glycolytic metabolism. A profound understanding of this mechanism can provide a clear mechanistic basis for the development of highly specific dye probes. It is worth noting that the cellular targeting of TCDs is not limited to OATP-mediated uptake of traditional small molecule dyes. Recently, Cy5 based supramolecular amino acid encoding nanodots have further demonstrated that the cyanine dye skeleton can also expand its cellular delivery function through nanoplatform design. This type of cyanine derived nanoplatform utilizes surface amino acid motifs to regulate protein recruitment, serum stability, and pH/ion responsive phase separation processes, achieving efficient and serum resistant cytoplasmic protein delivery [105]. It provides a new design approach for the functional expansion of TCDs in targeted delivery at the cellular level.

3.3 Organelle Targeting Specificity of TCDs

We summarized and analyzed the subcellular localization (as shown in **Table 1**), and the results showed that the vast majority of TCDs exhibited specific localization to mitochondria. Mitochondria are the core of cellular energy metabolism and the hub of cell apoptosis regulation, and their functional abnormalities are closely related to the occurrence and development of various diseases [106]. Therefore, developing mitochondrial-targeted compounds is a highly promising intervention strategy [107, 108]. Numerous studies have confirmed that mitochondrial targeting ability is a core functional attribute of TCDs [109]. Some studies have indicated that the mitochondrial membrane potential of tumor cells is higher than that of normal cells, which is the basis for the selective enrichment of the lipophilic cationic compound rhodamine 123 [110-113]. The mitochondrial targeting of TCD derivatives may not depend on the mitochondrial membrane potential, but rather achieved via energy-dependent or transporter-mediated pathways, thereby exhibiting diverse targeting mechanisms. Chen *et al*. confirmed that IR-780 can target mitochondria through stress induction. The preventive application of IR-780 can significantly inhibit the process of cell apoptosis triggered by ischemia and oxidative stress, thereby effectively maintaining cardiac function and delaying heart failure. Further mechanism analysis indicates that IR-780 induces a rapid decrease in mitochondrial membrane potential by specifically binding to F_0F_1-ATP synthase in the mitochondrial respiratory chain, thereby inhibiting energy metabolism and placing mitochondria in a "relative resting state". In addition, the compound can effectively inhibit the abnormal opening of the mitochondrial permeability transition pore (mPTP) by blocking mitochondrial calcium overload, exerting a cardioprotective effect [23].

Table 1. Representative TCDs classified by disease category and hierarchical targeting features.

Disease	TCDs	Structural features	Targeting mechanism	Hierarchical target	Off-target effects / selectivity limitations	Theranostic role	Biosafety	Ref
Tumor	Ph790H, DZ-1, Abi-DZ-1, FTS-148, IR-DBI, NIR-27, IR-34, IR-37, IR-58, IR-83, IR-783, IR-808DB, IR-808, IR-817, IR-780	Heterocyclic modification, Sulfonate, Carboxyl ester, Amino acid, Choline, Alkyl, 2-nitroimidazole, Abiraterone- or FTS-conjugated side chains	Mainly HIF-1α/OATP-mediated uptake; IR-780: OATP1B3 reported; DZ-1 in HCC: *OATP3A1/OATP4A1* implicated; mitochondrial membrane potential contributes to subcellular retention	Tumor tissue/Brain tumor/ GL261 tumor /Bladder tumor/ CSCs/CAFs → Cancer cells/Cancer stem-like cells or Stromal cells → Mitochondria/ Lysosomes/ER	OATP expression differs among tumor types and patients; possible uptake in normal OATP-expressing tissues; OATP subtype often not fully clarified	NIR tumor imaging, Tumor-targeted diagnosis, PTT/PDT, Drug delivery, Radiotherapy assistance, Immunotherapy, Tumor recurrence inhibition	Some dyes showed clearance from vital organs within 48 h; IR-783 showed long tumor retention; IR-34 showed two-phase half-life parameters	[28, 40, 44, 46, 51–53, 59, 61, 101, 112, 77-80, 114, 163, 164, 166, 146]
Fibrotic diseases	IR-780	Alkyl side chain	Glycolysis-dependent uptake; OATP subtype not specified; mitochondrial localization	Hypertrophic/Keloid scars/Granulation/ Lung → Fibroblasts/Activated fibroblasts → Mitochondria	Selectivity may depend on glycolytic activation state of fibroblasts; OATP subtype remains unclear	Imaging-guided PTT/PDT, Targeted fibroblast elimination, Antifibrotic intervention	–	[27, 96, 98]
Tumor associated fibroblasts	IR-780	Alkyl side chain	Preferential CAF uptake; mitochondrial accumulation; mechanism related to fibrotic phenotype and stromal metabolism, OATP subtype not specified	Tumor site → CAFs → Mitochondria	CAF heterogeneity may affect response; stromal-targeting selectivity needs validation across more tumor types	CAF-targeted theranostics; Tumor stroma modulation	–	[97]
Metabolic and inflammation diseases	IR-61	Heptamethine cyanine scaffold	Mitochondrial membrane potential-dependent accumulation; OATP subtype not reported	Visceral fat/ Bladder/Penis → Adipose tissue macrophages/Bladder smooth muscle cells or corpus cavernosum smooth muscle cells → Mitochondria	long-term metabolism and full off-target profile remain insufficiently defined	Anti-inflammatory regulation, Metabolic protection, Improvement of diabetic bladder dysfunction and erectile dysfunction	NIR fluorescence remained higher than that in other organs at 5 days in selected models	[29, 132, 125, 126]
Radiation-induced injuries	IR-ALN, IR-61, IR-780, IR-83	Aminophosphonate, sulfonate, Carboxybenzyl modification, Alkyl side chain or 2-nitroimidazole modification	Bone affinity and osteoclast precursor uptake for IR-ALN; mitochondrial targeting and Nrf2/HO-1 antioxidant regulation for IR-61; OATP involvement varies by dye and is often not subtype-defined	Bone/Lung/Bladder/Brain/Hematopoietic system / Tumor tissues under radiotherapy →Macrophages/Endothelial/Stem cells or tumor cells → Mitochondria	Bone-targeted retention and long-term clearance need evaluation; radiation injury models differ by organ	Protection against radiation-induced Bone loss, Lung injury, Cystitis, Brain injury, and hematopoietic injury; Radiotherapy enhancement	IR-ALN targets bone-related injury; IR-61 exerts antioxidant protection in RILI-related models	[22, 30, 52, 56, 128, 129]
Hematological malignancy	IR-26	Water-soluble amino acid ester side chain	Hyperactive glycolysis-dependent mitochondrial accumulation; OXPHOS inhibition; OATP subtype not reported	Leukemia cells → mitochondria	Selectivity may depend on AML metabolic state; off-target effects on other highly oxidative cells require evaluation	NIR imaging and leukemia-cell targeting	$t_{1/2}$ = 56.43 ± 6.38 h; Cmax = 115.23 ± 6.73 g/L; Tmax = 4 ± 1.73 h	[122]

Zhang *et al*. found that IR-780 can selectively localize to mitochondria after internalization, but its uptake mode is different from typical lipophilic cations. Even if 10 mM carbonyl cyanide-4-trifluoromethoxyphenylhydrazone (FCCP) induces mitochondrial depolarization, the internalization of IR-780 is still largely unaffected, indicating that mitochondrial membrane potential is not the main driving force for its accumulation [102]. In contrast, cyanine dyes such as IR-58 exhibit stronger mitochondrial selectivity. Huang *et al*. confirmed through Mito-Tracker Green co localization that IR-58 can target the mitochondria of HT-29 and HCT116 colorectal cancer cells (**Figure 6C**). Low temperature treatment and glycolysis or oxidative phosphorylation inhibitors significantly reduced its uptake, indicating that the mitochondrial enrichment of IR-58 depends on cellular metabolic energy supply [101]. Wang *et al*. reported that IR-780 can be enriched in mitochondria, and its uptake is closely related to the regulation of HIF-1α in cancer stem cells (CSCs). Upregulation of HIF-1α can enhance the activity of the mitochondrial

transporter *ABCB10*, thereby promoting the specific uptake of IR-780 (**Figure 6D**) [114]. Besides mitochondria, TCDs can also be used for endoplasmic reticulum (ER) targeting. ER-Cy-poNO_2 can preferentially accumulate in the ER of tumor cells and enhance the anti-tumor effect of PDT by inducing strong ER stress and immunogenic cell death (ICD) [115]. Chen *et al*. further encapsulated ER specific dyes in Ds-sP/TCPP-TER nanoparticles, which targeted ER under NIR irradiation and amplified ICD response by intensifying ER stress [116]. Some TCDs are not limited to a single organelle and have dual targeting capabilities. Ph790H can simultaneously locate in mitochondria and ER, and induce tumor cell death through mitochondrial damage, ROS generation, and ER stress [46]; Abi-DZ-1 targets mitochondria and lysosomes, promoting apoptosis and inhibiting tumor proliferation by disrupting mitochondrial function [78]. Therefore, the subcellular localization of TCDs not only supports their imaging and therapeutic effects, but also provides a basis for observing organelle related lesions and designing targeted therapies.

As shown in **Table 1**, the targeting characteristics of over 30 TCDs indicate that these dyes have practical value in the treatment of cancer, fibrosis, and metabolic diseases. Its mode of action can be summarized as "tissue-cell-subcellular": it is enriched in tumor or bone tissue at the tissue level, recognizes specific cell types such as fibroblasts at the cellular level, and is mainly localized in mitochondria (>90%) at the subcellular level. Some dyes also have dual targeting capabilities for mitochondria/lysosomes. This mitochondrial bias not only reflects its structural design characteristics, but also highlights the importance of mitochondrial regulation in treatment. **Table 1** further indicates that chemical structure fine-tuning can significantly affect the biological effects of TCDs. The skeleton of heptamethine mainly determines its color and basic targeting characteristics, while the side chain structure directly affects its water solubility, clearance rate, tumor retention, and mitochondrial affinity. Derivatives bearing sulfonic acid moieties, such as DZ-1 and IR-783 can improve water solubility and promote *in vivo* clearance. Derivatives functionalized with amphiphilic moieties, such as IR-DBI and IR-61 can help enhance tumor retention and mitochondrial binding. There are also differences in the distribution of different dyes in the body: IR-26 and IR-34 can maintain longer blood circulation, while most dyes have a clearance time of less than 48 hours in major organs such as the liver and kidneys. IR-783 shows good potential for guiding treatment due to its long-term retention in tumor tissues. Overall, these dyes have translational value in terms of safety and pharmacokinetics, but their long-term toxicity and specific metabolic pathways still need further clarification.

Overall, the differences between TCDs and squarylium/merocyanine dyes are not only in their NIR spectral performance, but also in their small molecular frameworks that can integrate multiple functions such as lesion enrichment, transporter mediated internalization, organelle localization, and therapeutic regulation [117]. Squarylium cyanine is highly attractive for stable NIR imaging and sensing, while merocyanine dyes exhibit excellent optical tunability and potential for NIR-II phototherapy [118]. However, their disease targeting often relies more on external functional modifications, nanocarrier construction, or responsive probe design [119]. In contrast, TCDs exhibit more significant structural associations and pathological targeting features. At the tissue level, selective accumulation can be achieved through passive EPR mediated retention and active ligand targeting. At the cellular level, the OATP-mediated transmembrane transport mechanism, which is closely related to hypoxia signaling and glycolysis reprogramming can achieve disease-related cell recognition. At the subcellular level, the specific localization of mitochondria (with minor distribution in lysosomes or ER) ensures the functional layout of therapeutic regulation. These collaborative mechanisms construct a hierarchical targeting mode of tissue/cell/organelle, enabling TCD design to accurately match the pathological microenvironment. Importantly, this targeted behavior is directly related to the synthesis and modification strategies described in chapter 2, which determine the targeting sequence, binding affinity, and stimulus response characteristics of TCDs. Therefore, the structure function synergy of TCDs provides a unique strategy to overcome the limited specificity of traditional diagnosis and treatment platforms, making them particularly suitable for hierarchical precision diagnosis and treatment.

4. Therapeutic Effects and Molecular Mechanisms of TCDs

4.1 Antioxidant and Cytoprotective Effects Mediated by the Nrf2 Pathway

As is well known, oxidative stress is a key driving factor for cell damage. Exposure to ionizing radiation (IR) or hydrogen peroxide (H_2O_2) can trigger the accumulation of large amounts of ROS within cells, resulting in DNA double-strand breaks (DSBs), apoptosis, tissue damage, and impaired self-healing ability [120, 121]. Given their intrinsic mitochondrial-targeting ability, TCDs can directly modulate

mitochondrial oxidative stress and protect cellular function. This property has contributed to their therapeutic effects in several oxidative stress-related disease models [122], as shown in the following specific cases.

NIRCP-61 has shown strong cell protective potential in preclinical studies. In the oxidative stress models induced by H_2O_2 and IR, NIRCP-61 can effectively alleviate damage to mesenchymal stem cells (MSCs). The results of the calcein AM/PI co-staining and colony formation experiments (**Figure 7A-B**) showed that NIRCP-61 pretreatment significantly reduced stress-induced cell death. The mechanism research results indicate that NIRCP-61 provides dual protection by reducing intracellular total ROS levels and decreasing IR-induced DNA damage, which is confirmed by the significant decrease in γ-H2AX expression (**Figure 7C**) [123]. This process can accelerate the dissociation of Nrf2 from its inhibitory partner protein Keap1, promote Nrf2 nuclear translocation, and thereby activate the transcriptional activity of downstream antioxidant response elements (AREs). At the same time, the increase in intracellular ROS levels can trigger activation of the PI3K/Akt pathway, which can further amplify antioxidant responses by promoting phosphorylation of Nrf2, Akt, and their negative regulatory factor GSK-3β [123, 124]. As shown in **Figure 7D**, Nrf2 activation upregulated antioxidant enzymes such as SOD1, SOD2, glutathione peroxidase-1 (GPX-1), and CAT, indicating that NIRCP-61 can enhance cellular antioxidant defense. Further animal experiments have shown that this protective effect is not limited to *in vitro* systems, but has also been validated in various *in vivo* models. For example, in a rat model of myocardial infarction, transplantation of human umbilical cord mesenchymal stem cells (hUCMSCs) pretreated with NIRCP-61 can significantly reduce the left ventricular infarct area. In addition, in the combined model of radiation injury and trauma injury, NIRCP-61 pretreatment accelerated wound healing on days 3 and 5 after injury (**Figure 7E**). Similarly, in a hindlimb injury model induced by high-dose radiation (40 Gy), NIRCP-61-pretreated hUCMSCs effectively improved skin ulcers and edema, and promoted dermal tissue regeneration (**Figure 7F**). Wang *et al*. further elucidated the potential molecular mechanism of IR-61 and pointed out that IR-61 can induce transient release of superoxide anions in mitochondria and cytoplasm [26]. Specifically, IR-61 preferentially enters adipose tissue macrophages (ATMs) and localizes to mitochondria. Via the ROS/Akt/Acly pathway, mitochondrial complexes and OXPHOS activity are enhanced, inhibiting M1 inflammatory activation, and improving obesity, insulin resistance, and fatty liver. This case demonstrates that TCDs can serve as immunometabolic modulators.

IR-61 exhibits a similar protective effect in the diabetic bladder dysfunction (DBD) model. Wang *et al*. found that IR-61 can alleviate mitochondria-associated apoptosis in the bladder tissues of DBD rats by inhibiting cellular and mitochondrial superoxide (MitoSOX) levels. Specifically, IR-61 treatment can significantly reverse downregulation of Nrf2, SOD-1, SOD-2, and HO-1 expression, while inhibiting Keap-1 upregulation in the bladder tissues of the DBD + IR-61 group, further confirming that the protective effects of IR-61 is closely related to the activation of the Nrf2 pathway [125]. A study conducted by Yue *et al*., focused on the injury of diabetes-related corpus cavernosum smooth muscle cell (CCSMC) associated with diabetes. The results showed that IR-61 could alleviate cellular and MitoSOX accumulation (**Figure 7G**), restore the protein levels of SIRT1 and SIRT3, and upregulate the expression of Nrf2 and HO-1 (**Figure 7H-I**), thereby reducing mitochondrial damage [126, 127]. Zheng *et al*. further confirmed in the radiation-induced RILI model that IR-61 alleviates oxidative stress and improves RILI by upregulating Nrf2 and its downstream antioxidant enzyme HO-1 in lung tissues. Specifically, IR-61 not only reduces inflammatory cell infiltration and IL-1β, IL-6, TNF-α, but also decreases fibrosis factors such as collagen I/III, α-SMA, and fibronectin. It is worth noting that IR-61 can also be enriched in the mitochondria of macrophages in irradiated lung tissue, ultimately achieving continuous protection through antioxidant/anti-inflammatory/antifibrotic [30]. IR-780, belonging to the same family of cyanine dyes, also exerts a strong cell protective effect through a similar oxidative stress regulation mechanism. Li *et al*. found that IR-780 pretreatment significantly reduces radiation-induced γ-H2AX expression in SV-HUC-1 cells, conferring cytoprotection by decreasing ROS accumulation and DSB damage; flow cytometry analysis confirmed concurrent upregulation of antioxidant enzymes (SOD1, SOD2, and CAT) [128]. Therefore, the application of IR-780 before radiation has great protective potential for preventing acute urinary tract mucosal injury and long-term bladder dysfunction. Zhang *et al*. further confirmed that IR-780 can be enriched in the mitochondria of damaged brain microvascular endothelial cells, reducing total intracellular ROS and MitoSOX levels in cerebral microvascular endothelial cells, thereby counteracting radiation-induced damage via oxidative stress modulation [129]. Therefore, this dye has the potential to protect neurovascular units and repair the BBB. Wu *et al*. further reported that IR-780 can specifically target

and enrich in long-acting hematopoietic stem cells with high mitochondrial membrane potential. By inducing cells to enter a resting state, IR-780 triggers an endogenous self-protection mechanism that not only significantly reduces ROS levels and the risk of DNA damage, but also effectively enhances the regenerative and hematopoietic recovery potential of stem cells. Based on this characteristic, applying IR-780 to preprocessing strategies is expected to become an efficient intervention method in the field of stem cell protection and radiation protection [22].

In conclusion, the mitochondria-targeted TCDs have good cellular protective effects under various oxidative stress-related pathological conditions, and their mechanism is mainly related to the activation of Nrf2 mediated antioxidant defense pathways. The research results confirm that such dyes not only potently reduce cellular and mitochondrial ROS levels and alleviate DNA damage, but also upregulate the expression of various antioxidant enzymes. In clinical models such as MSC protection, myocardial infarction, diabetes-related injuries and RII, TCDs consistently reverse cell death, reduce lesion size, and accelerate tissue repair, thus emerging as highly promising therapeutic candidates for oxidative stress-related diseases.

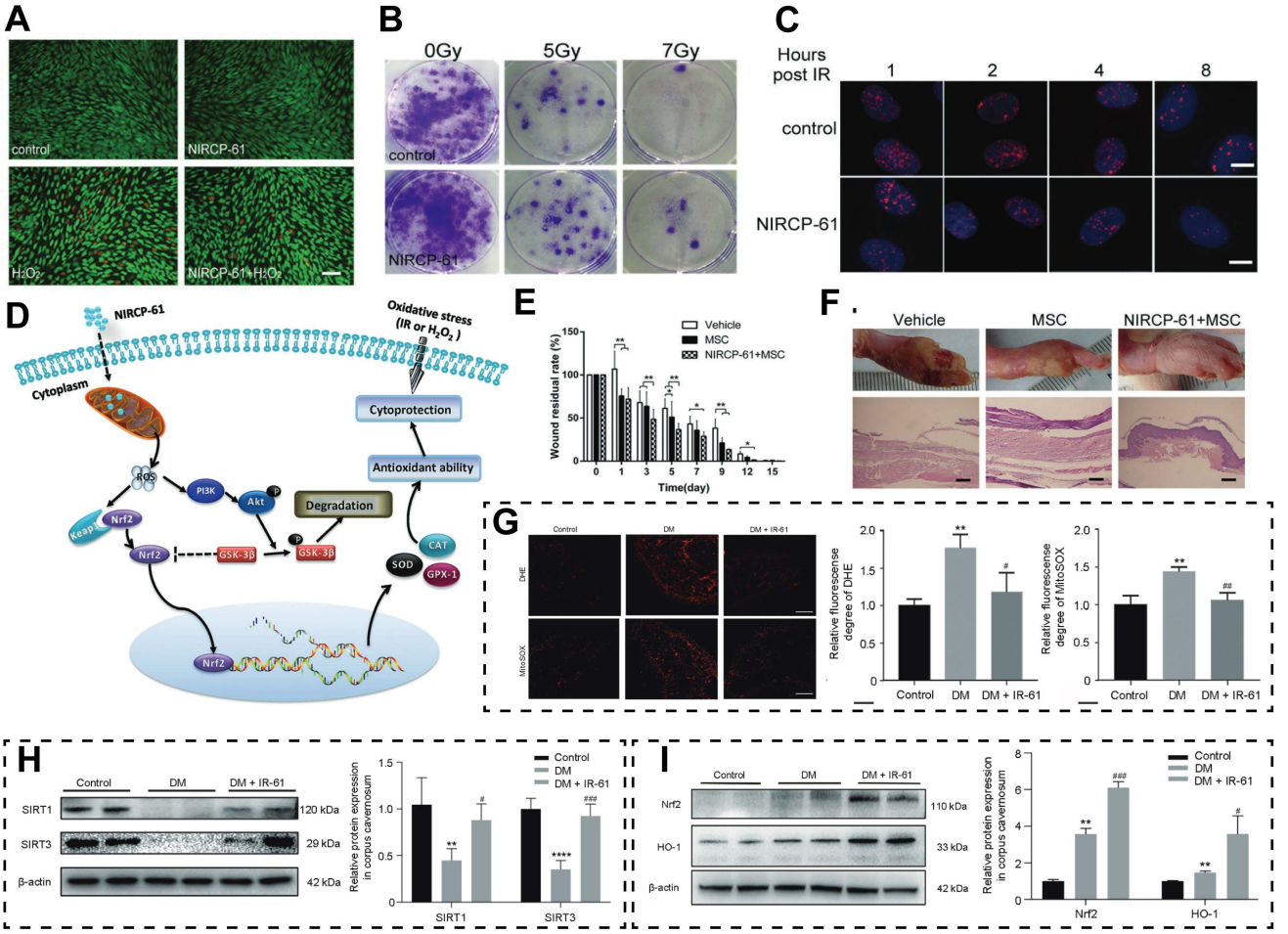

Figure 7. (A) The results of dual staining with calcein-AM and PI under different treatment conditions. (B) Images of hUCMSCs colony formation. (C) Images of γ-H2AX in the nuclei of hUCMSCs after IR. (D) Mechanisms of NIRCP-61 against oxidative stress. (E-F) The healing status of wounds at different time points. Adapted with permission from [123]. Copyright 2016, John Wiley and Sons. (G) DHE and MitoSOX staining and their quantitative results. (H) Representative images and quantitative results of Western blot analysis for SIRT1 and SIRT3. (I) Western blot analysis and quantification results of Nrf2 and HO-1 in tissues. Adapted with permission from [126]. Copyright 2025, Wolters Kluwer Medknow Publications.

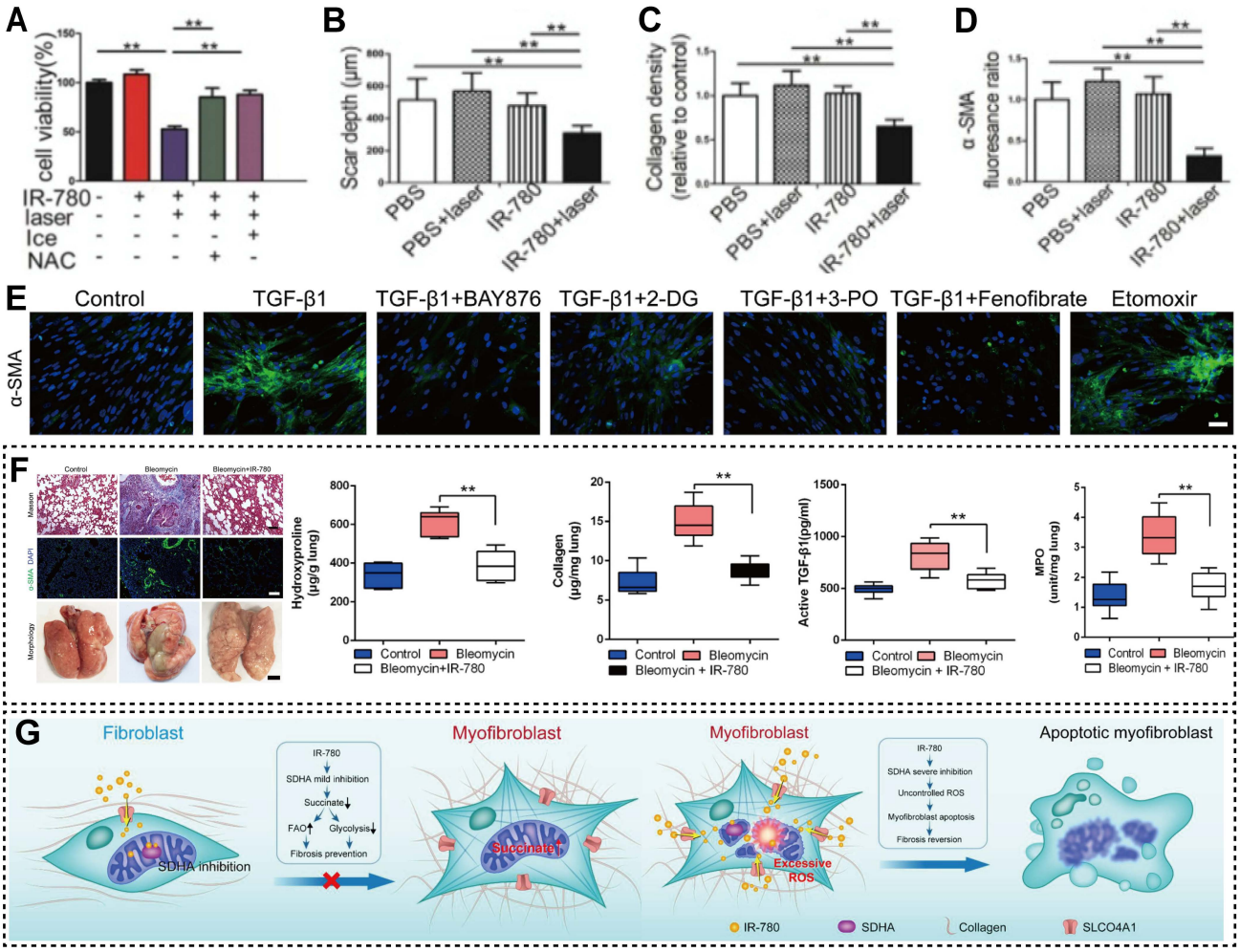

Figure 8. (A) Cell viability of primary fibroblasts treated with IR-780 under different treatment conditions. Analysis of scar depth (B), ECM deposition (C) and α-SMA (D) expression in healing wound tissues treated with IR-780. Adapted with permission from [27]. Copyright 2019, Ivyspring International Publisher. (E) Images and their quantification results of primary lung fibroblasts treated with different treatment groups. (F) Gross morphology and related indicators of the lungs of rats after 8 weeks of treatment. (G) Schematic diagram of the mechanism by which IR-780 controls lung fibrosis. Adapted with permission from [98]. Copyright 2019, Elsevier.

4.2 Antifibrotic Effects Mediated by Glycolysis

Tissue fibrosis constitutes a hallmark pathological feature of multiple diseases, including skin scarring, organ fibrosis, and tumor stroma formation, with the aberrant activation and proliferation of fibroblasts acting as the principal drivers of disease progression [130-132]. Fibroblasts can undergo metabolic reprogramming during fibrosis, exhibiting active aerobic glycolysis, which provides a basis for targeted interventions [133-135]. By utilizing the bias of TCDs towards metabolically abnormal cells, our team found that IR-780 can label glycolytic fibroblasts. Combined with directed laser irradiation, this type of pathological cells can be selectively killed. *In vitro* experiments have also confirmed that the mortality rate of IR-780 labeled cells is significantly higher than that of unlabeled controls. Calcein-AM/PI staining confirmed that the combination of PDT and PTT synergistically enhanced the photoinduced cytotoxicity of IR-780. The cell viability in the PDT-PTT combination group reached 52.6%, which was far lower than that in the PTT-alone group (85.2%) and the PDT-alone group (87.8%) (**Figure 8A**). *In vivo* experiments further verified that this phototherapy regimen can significantly reduce scar depth, extracellular matrix (ECM) deposition, and α-smooth muscle actin (α-SMA) expression (**Figure 8B-D**), thereby providing a novel approach for the intervention of excessive connective tissue deposition associated with wound healing [27]. Existing studies have demonstrated that radiation induces the activation of myofibroblasts, triggers an excessive tissue repair process, leads to ECM protein deposition, and thereby results in pulmonary fibrosis [136-138]. Furthermore, alveolar macrophages promote the transdifferentiation of fibroblasts and epithelial cells into myofibroblast-like cells, contributing to the progression of radiation-induced pulmonary fibrosis (RIPF) [139-141]. Therefore, Luo *et al*. found that

alveolar macrophages can also serve as therapeutic targets for pulmonary fibrosis. Treatment with IR-780 downregulates the expression levels of pro-fibrotic mRNAs in post-irradiation alveolar macrophages and the glycolysis inhibitor 2-deoxy-D-glucose also inhibits fibrosis development *in vitro* experiments, indicating that the antifibrotic effect of IR-780 is closely related to glycolysis regulation [142]. Wang *et al*. expanded the understanding of metabolic regulatory mechanisms, demonstrating that downregulation of fatty acid oxidation (FAO) and upregulation of glycolysis in fibroblasts jointly promote pulmonary fibrosis development. They further clarified that preferential inhibition of glycolysis provides greater advantages than FAO enhancement in antifibrotic therapy (**Figure 8E**). Additionally, they showed that IR-780 can block fibroblast transdifferentiation into myofibroblasts by preventing succinate accumulation and inhibiting HIF-1α activation. To explore the potential of IR-780, Wang *et al*. treated primary fibroblasts with transforming growth factor β1 (TGF-β1) and found that IR-780 significantly upregulated mRNA and protein levels of FAO-related molecules while simultaneously downregulating key factors in the glycolysis pathway. In rat models of bleomycin-induced pulmonary fibrosis, intraperitoneal injection of IR-780 improved lung tissue morphology, reduced lung collapse and fibrous nodules, and markedly decreased expression of fibrosis-related genes, including *TGF-β1*, collagen type I alpha 1 chain (*COL1A1*), connective tissue growth factor, matrix metalloproteinase 2, α-SMA, fibronectin, and plasminogen activator inhibitor 1. After an 8-week treatment course, IR-780 was shown to ameliorate established fibrotic lesions by selectively inducing myofibroblast apoptosis (**Figure 8F**) [98]. Based on previous studies, the preventive and therapeutic mechanisms of IR-780 in intervening bleomycin-induced pulmonary fibrosis have been clarified, namely that it moderately inhibits succinate dehydrogenase complex flavoprotein subunit A (*SDHA*) in normal fibroblasts and blocks the TGF-β1-mediated elevation of succinate dehydrogenase activity and succinate levels to prevent fibrosis formation and respiratory dysfunction, while potently inhibiting *SDHA* in myofibroblasts, triggering massive ROS production and further selectively inducing their apoptosis, ultimately achieving the amelioration of pulmonary fibrosis (**Figure 8G**) [98].

Hypertrophic scar (HS) is the most common complication following burns and trauma, and its core pathological feature is excessive fibrosis caused by aberrantly activated fibroblasts [143, 144]. Dysregulated glycolysis has been identified as a potential therapeutic target [133, 145]. Meng *et al*. demonstrated that the majority of α-SMA-positive fibroblasts in keloids exhibit hyperglycolytic characteristics, and fibroblast activation is closely correlated with enhanced glycolysis. Further experiments confirmed that IR-780 treatment can significantly downregulate the mRNA and protein expression levels of fibrosis-related factors, including α-SMA, *COL1A1*, and fibronectin in hypertrophic scar fibroblasts (HFs) and keloid fibroblasts (KFs), verifying that IR-780 inhibits the fibrotic activity of KFs by modulating the glycolysis pathway [96]. Increased abundance of CAFs is often associated with a poor prognosis, tissue stiffening, alterations in the immune-tolerant microenvironment, and other adverse events [146-148]. Taking advantage of the property of IR-780 to target fibrogenic fibroblasts, Yang *et al*. demonstrated that IR-780 could inhibit collagen secretion and induce CAF apoptosis. *In vivo* studies revealed that in EMT6 and MC38 xenograft models, IR-780 enhanced the anti-tumor efficacy of anti-PD-L1 therapy by reducing ECM protein deposition [97]. Zheng *et al*. found that IR-61 treatment alleviated radiation-induced collagen deposition and reduced hydroxyproline levels in lung tissues. Importantly, IR-61 also significantly downregulated the expression of fibrosis-related factors at both the mRNA and protein levels. During the 20-week post-irradiation observation period, the levels of pro-fibrotic cytokines, including Arg1, Fizz1, YM-1, TGF-β1, and PDGF, in lung tissues of rats in the IR-61 treatment group were significantly decreased, demonstrating long-term antifibrotic activity [30].

In conclusion, TCDs have made a series of advances in the treatment of fibrotic diseases due to their core characteristic of targeting glycolysis. TCDs can play a dual role in inhibiting fibroblast activation and inducing abnormal cell apoptosis, whether it is promoting fibrosis in fibroblasts or CAFs. These various fibrosis-related diseases provide predictable targeted treatment strategies and therefore have important clinical research value.

4.3 Multi-modal Synergistic Anti-tumor Effects of TCDs

4.3.1 Tumor Imaging and Therapy Mediated by TCDs

Functional materials with fluorescence properties have attracted increasing attention in the fields of sensing and imaging [108, 149, 150]. The latest research has achieved differentiated recognition of cancer cells through surface modification strategies using fluorescent metal cluster arrays, and further expanded the application scenarios of fluorescent materials in NIR biomedical fields through the construction of small molecule coupled nanoparticles

and optimization of NIR-II organic fluorescent cluster structures [151-153]. TCDs, with its outstanding deep tissue penetration and low fluorescence background advantages, has emerged as a key tool for tumor molecular imaging. It offers a wide range of technical support for early tumor detection, lesion localization, and curative effect monitoring [154-156]. In recent years, research on the integration of TCD diagnosis and therapy has become a leading trend in the field, and it has received extensive attention in the exploration of applications for precise tumor diagnosis and targeted intervention.

In the research of tumor imaging, NIR-27 has been proven to be capable of imaging a variety of tumor tissues, including gastric cancer MKN-45, lung cancer A549, and acute myeloid leukemia HL-60 tumor labeled with GFP [79]. As a widely used NIR dye, the imaging application of ICG has also been continuously optimized. Researchers have further confirmed that ICG can be internalized by differentiated HCC, enabling fluorescent imaging of tumor lesions [157, 158]. Owing to its superior optical characteristics and satisfactory biocompatibility, IR-780 has emerged as one of the most widely applied probes in bioimaging research [113]. Zhang *et al.* confirmed that IR-780, as an efficient tumor targeting agent, can stably emit light for more than 20 days to achieve long-term reliable imaging [77]. Its cellular uptake bypasses traditional endocytosis, mitochondrial voltage, or ATP-binding cassette transport pathways and instead depends on active energy metabolism, intact membrane potential, and normal OATP transporters [102].

Mitochondria, as the energy center that dominates cell death, are the main targets of TCDs for light-controlled signal intervention and tumor imaging [159-161]. Mechanism studies have shown that IR-780 can target the mitochondria of drug-resistant A549/DR cells, triggering apoptosis by enriching ROS and collapsing membrane potential [162]. IR-58, which has tumor selective toxicity, activates the TIM44-SOD2-ROS-mTOR axis, leading to excessive autophagy and programmed cell death [101]. Additionally, IR-37 exerts highly efficient killing of human colorectal cancer cells via the mitochondrial apoptotic pathway. In the *in vivo* HT-29 xenograft model in nude mice, tumor growth was significantly inhibited in the IR-37 treatment group. Subsequent mechanistic studies confirmed that the SOD1-ROS-JNK pathway, regulated by the positive cofactor 4, plays a central role in the apoptotic process [163]. Shen *et al*. first demonstrated that IR-780 interferes with electron transport by targeting mitochondria, leading to massive ROS production; when combined with hyperbaric oxygen, ROS further reduces mitochondrial membrane potential and exacerbates mitochondrial damage through a synergistic effect of oxygen (**Figure 9A**) [164].

TCDs are capable of eliciting anti-tumor effects by regulating ER stress or key signaling pathways. Wang *et al*. developed the probe IR-34, which can significantly inhibit the viability of various human tumor cell lines, including A549, HepG2, and MCF-7 (**Figure 9B**). *In vivo* experiments, intraperitoneal injection of IR-34 (three times per week) was shown to restrain tumor progression and postpone tumor recurrence (**Figure 9C**). Mechanistic studies revealed that IR-34 triggers tumor cell apoptosis by activating ER stress (**Figure 9D**) [28]. In addition to these mechanisms, the potential of TCDs to generate synergistic outcomes in tumor immunotherapy has drawn growing research interest. Meanwhile, increasing efforts have been devoted to exploring the capacity of IR-780 for ICD induction [165]. Related research by Jiang *et al*. validated that IR-780 can target mitochondria to destroy cancer cells, subsequently exposing tumor-associated antigens. This process eventually initiates ICD both *in vitro* and *in vivo*, and effectively inhibits tumor growth and metastasis. In the B16F10-OVA mouse model, the combined therapy of IR-780 and OT-1 T cells can significantly enhance the efficacy of adoptive T cell therapy (**Figure 9E-F**) [166].

Faced with the clinical challenges of strong drug resistance and high metastatic potential of melanoma, TCDs have achieved pivotal breakthroughs by virtue of their precise targeting and regulatory mechanisms. Sun *et al*. reported that IR-817 possesses strong anti-tumor potency toward typical melanoma cell lines such as A375 and B16-F10. Related mechanism analyses verified that IR-817 specifically targets the transcription factor E2F8. By regulating the E2F/Cyclin/CDK pathway, this compound triggers G0/G1 cell cycle arrest in tumor cells, and exhibits satisfactory anti-melanoma effects in both zebrafish and B16-F10 xenograft models [18]. Besides IR-817, ZWZ-3 inhibits the viability of B16 and A375 cells in a concentration and time-dependent manner, with IC_{50} values of 0.2 μM and 0.43 μM, respectively. Experimental evidence further shows that ZWZ-3 activates the mitochondrial apoptotic pathway by inducing intracellular accumulation of ROS. *In vivo* experiments showed that its tumor growth inhibition rate reached 76.3%, without significant body weight loss, thus verifying its potent efficacy and low toxicity [31]. Moreover, IR-418 can selectively enrich within melanoma cells and markedly restrict tumor cell proliferation *in vitro*. Molecular mechanistic analysis indicated that IR-418 suppresses melanoma growth via activation of the Bax/Bcl-2/cleaved caspase-

mediated mitochondrial apoptosis pathway. Meanwhile, it restrains melanoma metastasis by downregulating mitochondrial fission through the ERK/DRP1 signaling cascade [75]. IR-545 further expands the diversity of mechanisms of action. It can not only activate the mitochondrial-mediated endogenous apoptosis pathway by reducing the mitochondrial membrane potential, but also specifically inhibit the abnormal activation of PI3K/AKT/mTOR signaling pathway [74]. Notably, IR-546 plays an anti-tumor role by specifically inhibiting the transduction of the AKT/GSK3β signaling pathway [73].

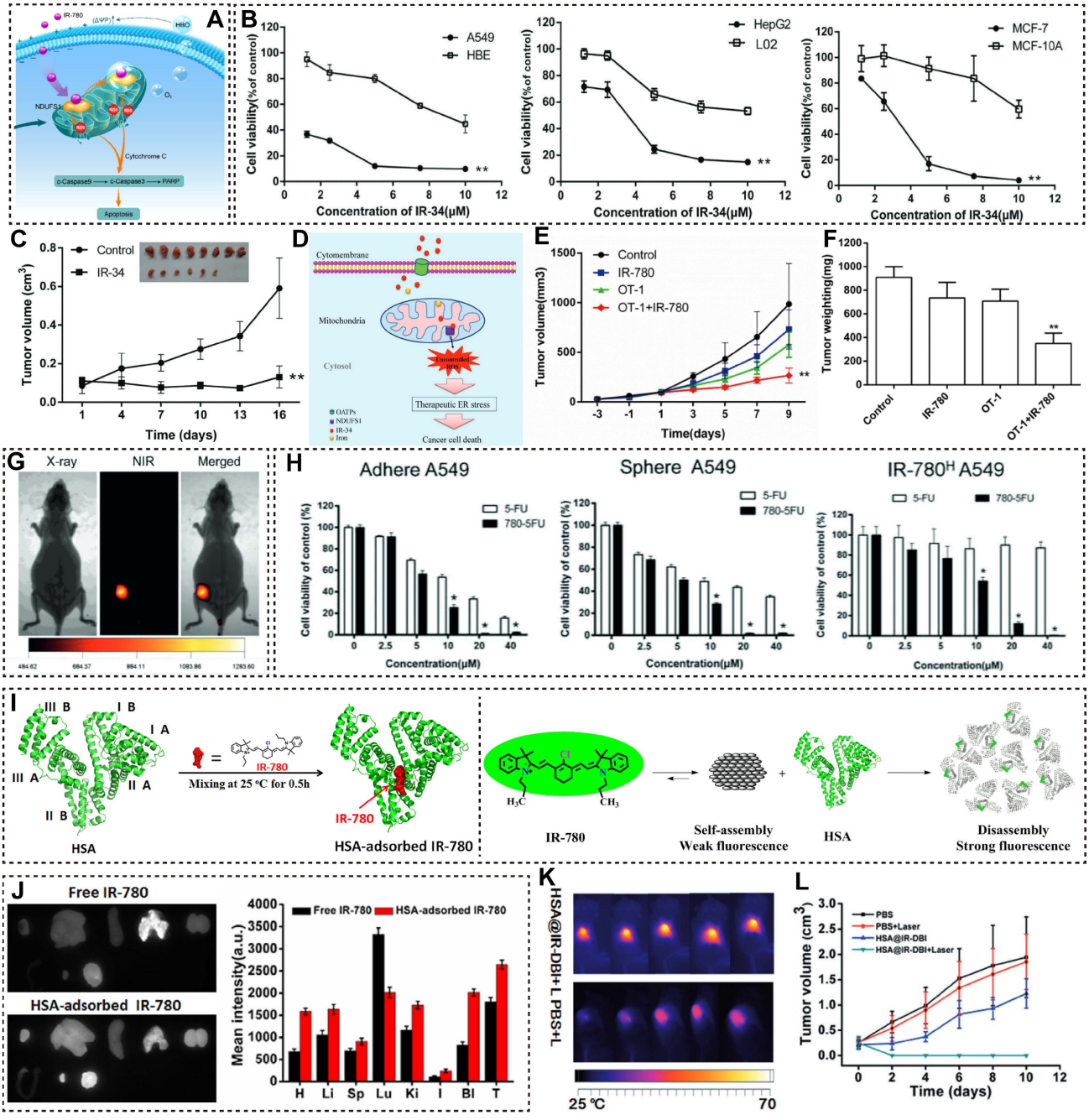

Figure 9. (A) Schematic diagram of the anti-tumor mechanism of IR-780 combined with hyperbaric oxygen. (B) The killing effect of IR-34 on different types of tumor cells. (C) Tumor volume change results of mice treated with IR-34. (D) The anti-tumor mechanism of IR-34. Adapted with permission from [28]. Copyright 2018, John Wiley and Sons. (E-F) Tumor volume and weight of different treatment groups. Adapted with permission from [166]. Copyright 2019, Frontiers Media. (G) Image results of 780-5FU in the nude mice. (H) Viability rate of cells in different states treated with 5-FU or 780-5FU. Adapted with permission from [114]. Copyright 2018, John Wiley and Sons. (I) Formation process of the IR-780/HSA complex and its fluorescence enhancement mechanism. (J) Imaging and quantitative results of anatomical organs in different groups of mice. Adapted with permission from [17]. Copyright 2022, BLACKWELL PUBLISHING INC. (K) Infrared thermal imaging results of tumor-bearing mice in the PBS and HSA@IR-DBI group. (L) Tumor volume results of different groups. Adapted with permission from [53]. Copyright 2017, John Wiley and Sons.

Although TCDs have achieved satisfactory results in the accurate diagnosis and treatment of tumors, they still have some shortcomings, including insufficient photostability, low PCE, and low biocompatibility. In order to solve this problem, Zhao *et al*. successfully synthesized the derivative T780T by introducing the TPE between two IR-780 molecules. The PCE of T780T reached 38.5%, which was significantly higher than that of free IR-780. *In vivo* experiments confirmed that after injecting T780T solution into the tail vein of 4T1 tumor-bearing mice, the NIR laser irradiation of the tumor site for 8 minutes could elevate the local temperature to over 52 °C, which confirmed that T780T had an excellent photothermal therapeutic effect [61].

4.3.2 Therapeutic Agent Delivery Mediated by TCDs

Endowed with tumor-targeting ability and biocompatibility, TCDs have emerged as ideal delivery carriers for therapeutic agents, such as chemotherapeutic drugs and radiosensitizers. Through the integrated design of targeted delivery, efficacy enhancement, and imaging guidance, these dyes effectively address the limitations of traditional therapeutic agents, including poor specificity, strong side effects, and insufficient bioavailability, thus significantly improving the precision and effectiveness of anti-tumor therapy. Jason Boyang Wu *et al*. confirmed that IR-783 can cross the BBB/BTB to accumulate in intracranial brain tumors and pituitary adenoma stem cell-like xenografts in mice. Based on this property, the researchers synthesized NIRG by conjugating IR-783 with gemcitabine. This conjugate exhibited a 7.9-fold higher accumulation in tumors than in other organs, and significantly inhibited tumor growth and metastasis [59]. IR-780 and nitrogen mustard conjugate IR-780NM have stronger anti-tumor potential [102]. To overcome the off-target toxicity and low targeting defects of 5-fluorouracil (5-FU) [167], Ang *et al.* linked 5-FU with IR-780 to construct 780-5FU. This fusion molecule can efficiently accumulate in the lesions of A549 tumor-bearing mice, and its anti-cancer effect is significantly better than using 5-FU alone (**Figure 9G, H**) [114].

Based on DZ-1 tumor targeting scaffolds, Zhang *et al*. and Qin *et al*. respectively developed NIRG and Abi-DZ-1 with dual effects of tumor specific imaging and growth inhibition/drug resistance reversal by coupling gemcitabine or abiraterone [51, 78]. Similarly, in response to the low solubility and bioavailability of the anticancer drug s-trans, trans-farnesylthiosalicylic acid (FTS), Zhao *et al*. connected it to MHI-148 to construct FTS-148. This hybrid molecule has excellent tumor selectivity, shows stronger antiproliferative activity than free FTS *in vivo* models of pancreatic cancer, and successfully overcomes its pharmacokinetic bottleneck [80].

In addition, TCDs can also achieve multi-modal synergistic therapy by integrating radio-sensitizing functions. Gao *et al*. incorporated 2-nitroimidazole, a classic radiosensitizer, into the IR-83 to construct a novel targeted molecule with both PTT and radio-sensitizing functions. Characterization results showed that the PCE of IR-83 reached 54.1%, which was significantly higher than that of most reported photothermal therapeutic materials. *In vitro* experiments confirmed that the tumor cell apoptosis rate in the IR-83 combined with NIR laser group was significantly increased to 62%, indicating that the combination strategy of IR-83 plus NIR laser effectively enhances X-ray-mediated tumor cell damage. *In vivo* experiments demonstrated that pretreatment with IR-83 and NIR laser significantly increased tumor cell radiosensitivity to IR [52]. Owing to its excellent photothermal performance, radio-sensitizing activity, and synergistic therapeutic potential, IR-83 is a highly promising candidate for a triple synergistic targeted therapy combining radiotherapy, PDT, and PTT against hypoxic tumors.

4.3.3 Anti-tumor Effects of Nanoparticles Mediated by TCDs

At present, nano-carriers have been proved to have good material advantages in many diseases. Numerous investigations have found that the assembly of nano-carriers and TCDs has potential in overcoming the inherent limitations of dyes and improving the effect of tumor targeted diagnosis and treatment. The main reason for this is that the carrier can protect TCDs in space, regulate their function and modify them in a targeted manner, so as to maximize the therapeutic effect of TCDs. For example, Long *et al*. conducted research on the interaction between TCDs and carrier HSA. The results of molecular docking showed that the binding site of IR-780 was located at the interface of IIA domain and IIB domain of HSA, and they formed a stable IR-780/HSA complex through non-covalent bonds. Experiments confirmed that the fluorescence intensity of IR-780/HSA complex was significantly better than that of free IR-780, mainly due to the fluorescence enhancement effect of IR-780 aggregate depolymerization induced by HSA (**Figure 9I**). In the 4T1 tumor-bearing mouse model, the fluorescence signal intensity of the IR-780/HSA complex at the tumor site was approximately 1.5 times that of free IR-780 (**Figure 9J**), which confirmed that the dye mediated by nano-carriers could enhance the performance of PTT [17]. Similarly, Tan *et al*. injected IR-DBI into the tail vein of 4T1 tumor-bearing mice, laser irradiation elevated the local tumor temperature

rapidly to 60 °C (**Figure 9K**), resulting in an excellent tumor inhibition effect (**Figure 9L**). This research again demonstrates that nano-carriers can increase the photothermal characteristics of dyes [53].

To address the issues of IR-817, such as poor water solubility, susceptible fluorescence quenching, insufficient efficacy in tumor-targeted imaging, and significant side effects, Wang *et al*. prepared BSA@IR-817 nanoparticles with a PCE of 32.6%, meeting the core performance requirements for PTT. In mouse models, the tumor growth inhibition rate of the group treated with BSA@IR-817 combined with laser irradiation exceeded 99% [20]. Shen *et al*. synthesized Cy750M-C1, but its poor water solubility limited its application. Therefore, they co-assembled Cy750M-C1 with DSPE-PEG_{2000} and DSPE-PEG_{2000}-FA via a two-step nanoprecipitation method to prepare Cy750M-C1-FA-NPs. Molecular mechanism studies demonstrated that Cy750M-C1 activates AMPK and promotes Drp1 dephosphorylation, mediates the translocation of Drp1 and BAX to mitochondria, induces mitochondrial fission and caspase activation, and ultimately triggers programmed apoptosis of tumor cells [65]. This study indicates that nanoassembly not only improves the water solubility and tumor delivery efficiency of TCDs, but also provides a foundation for their platform based functional expansion. Furthermore, in the collaborative therapy guided by photoacoustic imaging, IR-780@MPDA exhibits high drug loading capacity, enhanced tumor accumulation ability, and NIR fluorescence/photoacoustic dual-mode imaging characteristics. Under 808 nm laser irradiation, the platform achieved PDT/PTT combination therapy and induced ICD, increasing the infiltration rate of $CD3^+$ T cells to 40.6% and the proportion of $CD8^+$ cytotoxic T lymphocytes to 24.4%, revealing the potential association between TCD mediated phototherapy and anti-tumor immune activation [168]. In addition, a representative study, researchers screened molecular level precise Cy5 core polylysine G5 dendrimers with different peripheral amino acids to evaluate their ability to induce endocytosis, efflux, and cross cellular transport. Optimized nanodots can actively deliver therapeutic antibodies into solid tumors, enhance tumor penetration, and improve immune checkpoint blockade efficacy [169]. This suggests that through surface engineering and tree like macromolecular structure design, TCDs related platforms can not only achieve imaging and phototherapy, but also further undertake the active delivery function of macromolecular drugs.

4.3.4 Fluorescent Dendrimers as Complementary Platforms

In addition to small molecule TCDs, fluorescent dendritic macromolecules are an important class of macromolecular platforms that can further enhance the comprehensive diagnostic and therapeutic functions of cyanine dyes [170]. Dendritic macromolecules have highly branched structures, abundant terminal functional groups, and internal cavities, which can simultaneously load fluorescent dyes, targeted ligands, therapeutic drugs, and multimodal imaging components [171]. For integrated diagnostic and therapeutic formulations based on cyanines, coupling or encapsulation of dendritic macromolecules can enhance water solubility, photostability, local drug loading, *in vivo* circulation behavior, and multivalent targeting ability [172]. For example, studies have reported that dendritic nanoprobes labeled with Cy3/Cy5 can improve fluorescence brightness, photostability, and imaging localization accuracy, while nanohybrid materials based on dendritic macromolecules have been applied in molecular imaging, PDT, PTT, and integrated cancer diagnosis and treatment research fields [173]. Therefore, fluorescent dendritic macromolecules should be considered as complementary functional amplification platforms rather than substitutes for TCDs. Future research can combine the structural targeting ability of TCDs with the multivalent functionalization achieved by dendritic macromolecules to construct a hierarchical small molecule macromolecule hybrid diagnosis and treatment integrated system. However, its synthesis complexity, size dependent clearance properties, potential cationic toxicity, and potential impact on transporter mediated cellular uptake processes all require careful evaluation [174].

In summary, TCDs have the advantage of hierarchical targeting across tissues, cells, and subcellular levels. This enables them to show excellent adaptability in a variety of scenarios, especially with strong therapeutic potential in disease intervention. The above cases confirmed that TCDs performed well in antioxidation, cell protection, antifibrosis, and anti-tumor treatment. The main reason is closely related to its synthetic modification strategy and targeting mechanism. From the design of the structure to the assignment of targeting properties, the therapeutic effect has been clearly confirmed. In addition, the dendritic macromolecule platform can further enhance the water solubility, stability, targeting affinity, and theranostic integration ability of TCDs through modular modification and multivalent targeting, providing new functional amplification strategies for their clinical translation.

5. Summary and Outlook

With the in-depth advancement of the precision medicine concept, the development of novel molecular tools integrating high targeting capability and multi-modal theranostic functions has become an important research direction in the biomedical field. TCDs offer broad application prospects in disease diagnosis and therapy, owing to their excellent optical properties, tunable structural features, and favorable biocompatibility. This review systematically summarizes the design strategies, targeting and molecular mechanisms, and therapeutic applications of TCDs, highlighting their advantages in integrated diagnosis and treatment. Given the practical bottleneck of transitioning from basic research to clinical translation, future research needs to focus on tackling the following directions:

(1) Precision and intelligence guided molecular design: Introducing machine learning and quantitative SARs models in the early stages of development has become the mainstream trend for precise design of dye molecules, addressing application bottlenecks such as metabolic uncertainty and unexpected immune reactions. This type of calculation method can predict the liver and kidney clearance pathways and protein crown mediated immune risk in advance, thereby selectively screening candidates for *in vivo* trait optimization [175, 176]. In the field of stimulus responsive dyes, research is advancing towards finer logic control. The AND logic gate probe needs to simultaneously meet multiple microenvironment characteristics such as pH abnormality, specific enzyme expression, and tissue hypoxia in order to be activated. This "non lesion silencing" mechanism significantly reduces off-target effects and improves diagnostic safety [177-179].

(2) Photobleaching and photostability limitations: The photobleaching of TCD methylene chains under continuous laser irradiation is prone to fluorescence attenuation, which is the underlying bottleneck restricting their long-term imaging and phototherapy [180, 181]. This photodamage not only deteriorates the imaging quality, but also shortens the effective treatment window by inhibiting the sustained release of ROS and decreasing the PCE [182]. To this end, researchers have widely introduced modification methods such as cyanine structure modification, nano/supramolecular assembly, aggregation control, and dynamic fluorescence buffering [183-187], thus establishing a key path for building a highly stable integrated platform for diagnosis and treatment.

(3) Clinical translation and systems biology evaluation: The ultimate goal of bridging the barriers between pharmaceutical research and clinical application is to push TCDs to the forefront of clinical practice, including intraoperative tumor localization, capture of small residual lesions, and personalized treatment. However, this process is constrained by multiple factors, such as incomplete drug characteristics (metabolism and off-target accumulation), highly unreliable human EPR effects, and heterogeneity in the expression of transporters such as OATP. Therefore, there is an urgent need for bidirectional efforts in future research: on the one hand, introducing active/stimulus response mechanisms at the chemical source to deconstruct passive delivery defects, and on the other hand, conducting rigorous ADME/Tox evaluations at the biological end using physiological related models such as organoids and humanized mice to obtain reliable toxicological data [188, 189].

(4) Integration of multi-modal theranostic technologies: In response to the inherent limitations of deep tissue penetration in TCD imaging, positron emission isotopes are used to directly radio-label the stent without chelating agents, ensuring highly synchronized biological distribution and clearance dynamics between optical and PET signals [190, 191]. In terms of treatment, overcoming tumor drug resistance and immune evasion is currently the core of clinical practice. Reasonably designed TCD mediated PDT can reverse the immune "cold" tumor state by triggering ICD cascade reactions to release tumor associated antigens and reshape the immunosuppressive microenvironment, resulting in significant synergistic effects with immune checkpoint inhibitors [188, 192].

(5) Expansion of disease application scope: Relying on its unique photophysical properties, the application of TCDs is extending from oncology to dynamic physiological monitoring of non-malignant lesions. Overcoming heterogeneous biological barriers is key to deepening this field: for neurodegenerative diseases, precise regulation of scaffold lipophilicity, topological polarity surface area, and molecular weight can efficiently penetrate the BBB, enabling specific detection of early β-amyloid or tau protein aggregates. In fibrosis and metabolic disease models, rationally designed TCDs focus on identifying fibroblast activation proteins or quantifying local ROS fluctuations [193, 194]. Ultimately, such precise structural customization empowers TCDs to deliver quantifiable, molecular-level diagnostics for chronic conditions that routinely evade detection by conventional imaging.

In summary, TCDs, as a promising class of integrated diagnostic and therapeutic molecular tools, have demonstrated outstanding performance and

potential. In future research, the relationship between structure and function should be continuously explored, and *in vitro* and *in vivo* evaluation systems should be improved. Only in this way can TCDs have the potential to further improve the effectiveness of clinical diagnosis and treatment. Ultimately, providing innovative solutions for personalized diagnosis and treatment of human diseases.

Abbreviations

α-SMA: α-smooth muscle actin; ALN: alendronate sodium; AREs: antioxidant response elements; ALP: alkaline phosphatase; BBB: blood-brain barrier; BSA: bovine serum albumin; BTB: blood-tumor barrier; CAFs: cancer-associated fibroblasts; CAT: catalase; *COL1A1*: collagen type I alpha 1 chain; CSCs: cancer stem cells; D-A: donor-acceptor; DSBs: double-strand breaks; DMF: dimethylformamide; PDT: photodynamic therapy; ECM: extracellular matrix; EPR: enhanced permeability and retention; ER: endoplasmic reticulum; FAO: fatty acid oxidation; FCCP: carbonyl cyanide-4-trifluoromethoxyphenylhydrazone; FTS: s-trans, trans-farnesylthiosalicylic acid; GPX-1: glutathione peroxidase-1; HO-1: heme oxygenase-1; HCC: hepatocellular carcinoma cells; H_2O_2: hydrogen peroxide; HIF-1α: hypoxia-inducible factor-1α; HFs: hypertrophic scar fibroblasts; HSA: human serum albumin; hUCMSCs: human umbilical cord mesenchymal stem cells; ICD: immunogenic cell death; ICG: indocyanine green; IR: ionizing radiation; KFs: keloid fibroblasts; MitoSOX: mitochondrial superoxide; MSCs: mesenchymal stem cells; NIR: near-infrared; NM: nitrogen mustard; OATPs: organic anion transporting polypeptides; PCE: photothermal conversion efficiency; $POCl_3$: phosphorus oxychloride; PTT: photothermal therapy; RILI: radiation-induced lung injury; RIPF: radiation-induced pulmonary fibrosis; ROS: reactive oxygen species; SISE: stress-induced selective enrichment; SARs: structure-activity relationships; *SDHA*: succinate dehydrogenase complex flavoprotein subunit A; *SLCO*: solute carrier organic anion transporter polypeptide superfamily; TGF-β1: transforming growth factor β1; TCDs: targeting cyanine dyes; TPE: tetraphenylethylene; 5-FU: 5-fluorouracil.

Acknowledgments

This work was supported by Major Program from National Natural Science Foundation of China (82192884). The artificial intelligence tool ChatGPT was solely employed for grammatical refinement during manuscript preparation. The authors have independently verified all content and assume full responsibility for the integrity of the final publication. No AI technologies were used for data collection, analysis, or image generation.

Author contributions

Shuai Zhang: Writing-original draft & editing. Yang Xu: Writing-original draft. Yu Wang: Conceptualization, Supervision. Zelin Chen: Supervision. Yang Wang: Supervision. Quanying Liu, Tantan Wang, and Yali Dai revised the manuscript critically for important intellectual content. Chunmeng Shi: Writing-review & editing, Supervision, Funding acquisition.

Competing Interests

The authors have declared that no competing interest exists.

References

1. Awwad O, Ahram M, Coperchini F, Jalil MA. Precision medicine: recent advances, current challenges and future perspectives. Front Pharmacol. 2024; 15: 1439276.
2. Daryanani A, Turkbey B. Recent advancements in CT and MR imaging of prostate cancer. Semin Nucl Med. 2022; 52: 365-73.
3. Petzschner FH. Practical challenges for precision medicine. Science. 2024; 383: 149-50.
4. Pulumati A, Pulumati A, Dwarakanath BS, Verma A, Papineni RV. Technological advancements in cancer diagnostics: Improvements and limitations. Cancer Rep. 2023; 6: e1764.
5. Yuan B. What personalized medicine humans need and way to it-also on the practical significance and Scientific Limitations of Precision Medicine. Pharmgenomics Pers Med. 2022: 927-42.
6. Hauner K, Maisch P, Retz M. Side effects of chemotherapy. Urologe A. 2017; 56: 472-9.
7. Henderson NC, Rieder F, Wynn TA. Fibrosis: from mechanisms to medicines. Nature. 2020; 587: 555-66.
8. Kriebs A. Accumulation of macrophages in adipose tissue. Nat Rev Endocrinol. 2021; 17: 4-4.
9. Li S, Wang P, Liu Y, Yang K, Zhong R, Cheng D, *et al*. A mitochondrial-targeted near-infrared fluorescent probe for visualizing the fluctuation of hypochlorite acid in idiopathic pulmonary fibrosis mice. Anal Chim Acta. 2023; 1239: 340731.
10. Bedocchi O, Polena J, Okoročenkova J, Slavíček P, Klán P. Engineering the Photophysics of Cyanines by Chain C1′ Substituents. J Org Chem. 2025; 90: 17797-17813.
11. Kulinich AV, Ishchenko AA. Merocyanines: electronic structure and spectroscopy in solutions, solid state, and gas phase. Chem Rev. 2024; 124: 12086-144.
12. Yuan J, Yang H, Huang W, Liu S, Zhang H, Zhang X, *et al*. Design strategies and applications of cyanine dyes in phototherapy. Chem Soc Rev. 2025; 54, 341-366.
13. Zhu J, He G, Chen P-H, Zhang Y, Zhang Y, Lei S, *et al*. Terpyridine-grafted nitrogen-terminal endowing cyanine with metal-ion-regulated photophysical properties for cancer theranostics. Research. 2023; 6: 0061.
14. Zhang L, Jia H, Liu X, Zou Y, Sun J, Liu M, *et al*. Heptamethine cyanine–based application for cancer theranostics. Front Pharmacol. 2022; 12: 764654.
15. Shi C, Zhu Y, Cheng T, Su Y. Effective targeting, imaging and photodynamic killing of cancer cells with a new class of heptamethine 3H-indocyanine dyes. EXPERIMENTAL HEMATOLOGY: ELSEVIER SCIENCE INC 360 PARK AVE SOUTH, NEW YORK, NY 10010-1710 USA; 2008. p. S50-S.
16. Kootala S, Ossipov D, van den Beucken JJ, Leeuwenburgh S, Hilborn J. Bisphosphonate-functionalized hyaluronic acid showing selective affinity for osteoclasts as a potential treatment for osteoporosis. Biomater Sci. 2015; 3: 1197-207.
17. Long L, Tan X, Liu Z, Liu Y, Cao X, Shi C. Effects of Human Serum Albumin on the Fluorescence Intensity and Tumor Imaging Properties of IR-780 Dye. Photochem Photobiol. 2022; 98: 935-44.
18. Sun C, Wang J, Xia T, Sun Q, He Y, Wang H, *et al*. Mitochondrion-Targeted NIR therapeutic agent suppresses melanoma by inducing apoptosis and cell cycle arrest via E2F/Cyclin/CDK pathway. Pharmaceuticals. 2022; 15: 1589.
19. Fang J, Nakamura H, Maeda H. The EPR effect: unique features of tumor blood vessels for drug delivery, factors involved, and limitations and augmentation of the effect. Adv Drug Deliv Rev. 2011; 63: 136-51.

20. Wang J, Liao H, Ban J, Li S, Xiong X, He Q, *et al*. Multifunctional near-infrared dye IR-817 encapsulated in albumin nanoparticles for enhanced imaging and photothermal therapy in melanoma. Int J Nanomedicine. 2023; 18:4949-4967.
21. Hagenbuch B, Stieger B, Locher KP. Organic anion transporting polypeptides: Pharmacology, toxicology, structure, and transport mechanisms. Pharmacol Rev. 2025; 77: 100023.
22. Wu J, Ma L, Gong Q, Chen Y, Chen L, Shi C. Near-Infrared Dye Ir-780 Alleviates Hematopoietic System Damage by Promoting Hematopoietic Stem Cells into Quiescence. Shock. 2024; 61: 442-53.
23. Chen Z, Tan X, Jin T, Wang Y, Dai L, Shen G, *et al*. Pharmaceutical manipulation of mitochondrial F0F1-ATP synthase enables imaging and protection of myocardial ischemia/reperfusion injury through stress-induced selective enrichment. Adv Sci. 2024; 11: 2307880.
24. Pi F, Yan B, Jia M, Liu Y, Tang S, Huang Z, *et al*. IR-780 improves urination function and complications in rats with partial bladder outlet obstruction by protecting bladder smooth muscle cell mitochondria from oxidative stress. Front Pharmacol. 2026; 17: 1778496.
25. Li Y, Bai X, Yang D. Development and Application of Cationic Nile Blue Probes in Live-Cell Super-Resolution Imaging and Specific Targeting to Mitochondria. ACS Cent Sci. 2024; 10: 1221-30.
26. Xu W, Teoh CL, Peng J, Su D, Yuan L, Chang Y-T. A mitochondria-targeted ratiometric fluorescent probe to monitor endogenously generated sulfur dioxide derivatives in living cells. Biomaterials. 2015; 56: 1-9.
27. Chen Z, Wang Z, Jin T, Shen G, Wang Y, Tan X, *et al*. Fibrogenic fibroblast-selective near-infrared phototherapy to control scarring. Theranostics. 2019; 9: 6797.
28. Wang Y, Luo S, Zhang C, Liao X, Liu T, Jiang Z, *et al*. An NIR-Fluorophore-Based Therapeutic Endoplasmic Reticulum Stress Inducer. Adv Mater. 2018; 30: 1800475.
29. Wang Y, Tang B, Long L, Luo P, Xiang W, Li X, *et al*. Improvement of obesity-associated disorders by a small-molecule drug targeting mitochondria of adipose tissue macrophages. Nat Commun. 2021; 12: 102.
30. Zheng J, Wang Y, Wang Z, Chen W, Luo M, Zhang C, *et al*. Near-infrared Nrf2 activator IR-61 dye alleviates radiation-induced lung injury. Free Radic Res. 2022; 56: 411-26.
31. Liu Z, Wang H, Sun C, He Y, Xia T, Wang J, *et al*. ZWZ-3, a fluorescent probe targeting mitochondria for melanoma imaging and therapy. Front Pharmacol. 2022; 13: 829684.
32. A Shindy H. Basics, mechanisms and properties in the chemistry of cyanine dyes: a review paper. Mini Rev Org Chem. 2012; 9: 352-60.
33. Mishra A, Behera RK, Behera PK, Mishra BK, Behera GB. Cyanines during the 1990s: a review. Chem Rev. 2000; 100: 1973-2012.
34. Shindy H. Fundamentals in the chemistry of cyanine dyes: A review. Dyes Pigm. 2017; 145: 505-13.
35. Wang S, Tang Q, Ya H, Fan Y, Feng W, Du J, *et al*. Study on the optical and biological properties in vitro of IR808-PEG-FA. J Biomed Mater Res A. 2020; 108: 1816-23.
36. Zhang C, Tan X, Tan L, Liu T, Liu D, Zhang L, *et al*. Labeling stem cells with a near-infrared fluorescent heptamethine dye for noninvasive optical tracking. Cell Transplant. 2011; 20: 741-51.
37. Youn H-S, Park S-Y, Shin S-R, Shin J-I, Oh S-G, Jun K, *et al*. Design and synthesis of novel symmetrical heptamethine cyanine chromophores. Fibers Polym. 2010; 11: 321-3.
38. Li DH, Schreiber CL, Smith BD. Sterically shielded heptamethine cyanine dyes for bioconjugation and high performance near-infrared fluorescence imaging. Angew Chem. 2020; 132: 12252-9.
39. Shi X, Jung Y, Lin L-J, Liu C, Wu C, Cann IK, *et al*. Quantitative fluorescence labeling of aldehyde-tagged proteins for single-molecule imaging. Nat Methods. 2012; 9: 499-503.
40. Li DH, Gamage RS, Oliver AG, Patel NL, Muhammad Usama S, Kalen JD, *et al*. Doubly Strapped Zwitterionic NIR-I and NIR-II Heptamethine Cyanine Dyes for Bioconjugation and Fluorescence Imaging. Angew Chem. 2023; 135: e202305062.
41. He B, Wang Z, Sun Y, Piao Y, Dong C, Shen Y, *et al*. Dendritic NIR-II Cyanines Enable Deep Imaging and Precise Surgery. Small. 2025; 21: e09826.
42. Tan X, Luo S, Wang D, Su Y, Cheng T, Shi C. A NIR heptamethine dye with intrinsic cancer targeting, imaging and photosensitizing properties. Biomaterials. 2012; 33: 2230-9.
43. Lv Q, Yang X, Wang M, Yang J, Qin Z, Kan Q, *et al*. Mitochondria-targeted prostate cancer therapy using a near-infrared fluorescence dye-monoamine oxidase A inhibitor conjugate. J Control Release. 2018; 279: 234-42.
44. Luo S, Tan X, Qi Q, Guo Q, Ran X, Zhang L, *et al*. A multifunctional heptamethine near-infrared dye for cancer theranosis. Biomaterials. 2013; 34: 2244-51.
45. Panigrahi M, Dash S, Patel S, Mishra BK. Syntheses of cyanines: a review. Tetrahedron. 2012; 68: 781-805.
46. Park Y, Yang J, Kim MS, Hyun H. A Three-In-One Heptamethine Cyanine Dye Induces Endoplasmic Reticulum Stress and Apoptosis in Colorectal Cancer. Adv Healthc Mater. 2025; 14: 2404027.
47. Lim W, Byun JY, Jo G, Kim EJ, Park MH, Hyun H. Molecular Tuning of IR-786 for Improved Tumor Imaging and Photothermal Therapy. Pharmaceutics. 2022; 14: 676.
48. Zeng S, Liu L, Cheng Q, Chen W, Wang M, Wu M, *et al*. Novel Mitochondria-Targeted asymmetric heptamethine cyanine dye for Cancer targeted NIR imaging and potent necrosis and senescence induction with prolonged retention. J Med Chem. 2025; 68: 8174-89.
49. Tian Y, Chen Z, Liu S, Wu F, Cao W, Pang DW, *et al*. "Dual-Key-and-Lock" NIR-II NSCyanines Enable High-Contrast Activatable Phototheranostics in Extrahepatic Diseases. Angew Chem. 2023; 135: e202309768.
50. Leitão MM, de Melo-Diogo D, Alves CG, Lima-Sousa R, Correia IJ. Prototypic heptamethine cyanine incorporating nanomaterials for cancer phototheragnostic. Adv Healthc Mater. 2020; 9: 1901665.
51. Zhang C, Zhao Y, Zhang H, Chen X, Zhao N, Tan D, *et al*. The application of heptamethine cyanine dye DZ-1 and indocyanine green for imaging and targeting in xenograft models of hepatocellular carcinoma. Int J Mol Sci. 2017; 18: 1332.
52. Gao M, Huang X, Wu Z, Wang L, Yuan S, Du Z, *et al*. Synthesis of a versatile mitochondria-targeting small molecule for cancer near-infrared fluorescent imaging and radio/photodynamic/photothermal synergistic therapies. Mater Today Bio. 2022; 15: 100316.
53. Tan X, Luo S, Long L, Wang Y, Wang D, Fang S, *et al*. Structure-guided design and synthesis of a mitochondria-targeting near-infrared fluorophore with multimodal therapeutic activities. Adv Mater. 2017; 29: 1704196.
54. Li J, Yao P. Self-assembly of ibuprofen and bovine serum albumin-dextran conjugates leading to effective loading of the drug. Langmuir. 2009; 25: 6385-91.
55. Taboada P, Gutiérrez-Pichel M, Mosquera V. Effects of the molecular structure of two amphiphilic antidepressant drugs on the formation of complexes with human serum albumin. Biomacromolecules. 2004; 5: 1116-23.
56. Long L, Wu F, Li H, Cao X, Wang Y, Tan X, *et al*. Phosphonated Heptamethine Dye Alleviates Radiation-Induced Bone Loss. Adv Ther. 2024; 7: 2300287.
57. Guo Q, Luo S, Qi Q, Shi C. Preliminary Structure-Activity Relationship Study of Heptamethine Indocyanine Dyes for Tumor-Targeted Imaging. J Innov Opt Health Sci. 2013; 6: 1350003.
58. Liu Y, Zhou J, Wang L, Hu X, Liu X, Liu M, *et al*. A cyanine dye to probe mitophagy: simultaneous detection of mitochondria and autolysosomes in live cells. J Am Chem Soc. 2016; 138: 12368-74.
59. Wu JB, Shi C, Chu GC-Y, Xu Q, Zhang Y, Li Q, *et al*. Near-infrared fluorescence heptamethine carbocyanine dyes mediate imaging and targeted drug delivery for human brain tumor. Biomaterials. 2015; 67: 1-10.
60. Meng X, Li W, Sun Z, Zhang J, Zhou L, Deng G, *et al*. Tumor-targeted small molecule for dual-modal imaging-guided phototherapy upon near-infrared excitation. J Mater Chem B. 2017; 5: 9405-11.
61. Zhao X, Zhao H, Wang S, Fan Z, Ma Y, Yin Y, *et al*. A tumor-targeting near-infrared heptamethine cyanine photosensitizer with twisted molecular structure for enhanced imaging-guided cancer phototherapy. J Am Chem Soc. 2021; 143: 20828-36.
62. Gogvadze V, Orrenius S, Zhivotovsky B. Mitochondria as targets for cancer chemotherapy. Semin Cancer Biol. 2009; 19: 57-66.
63. Guan F, Wu X, Zhou J, Lin Y, He Y, Fan C, *et al*. Mitochondrial transfer in tunneling nanotubes-a new target for cancer therapy. J Exp Clin Cancer Res. 2024; 43: 147.
64. Lu H, Tong W, Jiang M, Liu H, Meng C, Wang K, *et al*. Mitochondria-targeted multifunctional nanoprodrugs by inhibiting metabolic reprogramming for combating cisplatin-resistant lung cancer. ACS nano. 2024; 18: 21156-70.
65. Shen Z, Zhang F, Yang J, Zhang K, Liang F, Mu H, *et al*. Novel Mitochondria-Targeted NIR Cyanine Cy750M-C1 Nanoparticles for Chemotherapy against Triple-Negative Breast Cancer. ACS Biomater Sci Eng. 2025; 11: 3738-51.
66. Han X, Song X, Yu F, Chen L. A ratiometric near-infrared fluorescent probe for quantification and evaluation of selenocysteine-protective effects in acute inflammation. Adv Funct Mater. 2017; 27: 1700769.
67. Siriwibool S, Kaekratoke N, Chansaenpak K, Siwawannapong K, Panajapo P, Sagarik K, *et al*. Near-Infrared Fluorescent pH Responsive Probe for Targeted Photodynamic Cancer Therapy. Sci. Rep. 2020; 10: 1283.
68. Zong Q, Zheng R, Xiao X, Jiang M, Li J, Yuan Y. Dual-locking nanoprobe based on hemicyanine for orthogonal stimuli-triggered precise cancer imaging and therapy. J Control Release. 2021; 338: 307-15.
69. Gao Z, Sun J, Gao M, Yu F, Chen L, Chen Q. A unique off-on near-infrared cyanine-based probe for imaging of endogenous alkaline phosphatase activity in cells and in vivo. Sens Actuators B Chem. 2018; 265: 565-74.
70. Liu Y, Teng L, Lou X-F, Zhang X-B, Song G. "Four-in-one" design of a hemicyanine-based modular scaffold for high-contrast activatable molecular afterglow imaging. J Am Chem Soc. 2023; 145: 5134-44.
71. Wang X, Wang H, Duan J, Sun Q, Zhang C, Xu L, *et al*. Phenothiazine-hemicyanine hybrid as a near-infrared fluorescent probe for ratiometric imaging of hypochlorite in vivo. Sens Actuators B Chem. 2024; 407: 135453.
72. Xu S-L, Guo F-F, Xu Z-H, Wang Y, James TD. A hemicyanine-based fluorescent probe for ratiometric detection of ClO-and turn-on detection of viscosity and its imaging application in mitochondria of living cells and zebrafish. Sens Actuators B Chem. 2023; 383: 133510.
73. Liao H, Xia T, Zeng Z, Yang X, Yang S, Xiong X, *et al*. Novel NIR fluorescent probe IR-546 inhibits melanoma through the AKT/GSK3β/β-catenin pathway. Mol Med. 2025; 31: 226.
74. Xia T, Liao H, Zeng Z, Li M, Yang S, Yang X, *et al*. A Dual-Functional Mitochondrial Probe for Melanoma Visualization and PI3K/AKT/mTOR-EMT Signaling Axis-Mediated Antitumor Therapy. Colloids Surf B Biointerfaces. 2025; 254: 114847.

75. He Q, Li C, Ou Y, Pan Y, Yang X, Wang J, *et al*. A novel NIR fluorescent probe inhibits melanoma progression through apoptosis and ERK/DRP1-mediated mitochondrial fission. Bioorg Chem. 2024; 145: 107218.
76. Yang J, Wang K, Zheng Y, Piao Y, Wang J, Tang J, *et al*. Molecularly precise, bright, photostable, and biocompatible cyanine nanodots as alternatives to quantum dots for biomedical applications. Angew Chem. 2022; 134: e202202128.
77. Zhang C, Liu T, Su Y, Luo S, Zhu Y, Tan X, *et al*. A near-infrared fluorescent heptamethine indocyanine dye with preferential tumor accumulation for in vivo imaging. Biomaterials. 2010; 31: 6612-7.
78. Qin J, Zhang C, Zhao Y, Tan D, Wu P, Shui X, *et al*. Small Mitochondria-Targeting Fluorophore with Multifunctional Therapeutic Activities against Prostate Cancer via the HIF1α/OATPs Pathway. Mol Pharm. 2023; 20: 6226-36.
79. Liu T, Luo S, Wang Y, Tan X, Qi Q, Shi C. Synthesis and characterization of a glycine-modified heptamethine indocyanine dye for in vivo cancer-targeted near-infrared imaging. Drug Des Devel Ther. 2014; 8: 1287-97.
80. Zhao Y, Zhang H, Wu P, Tan D, Zhao Y, Zhang C, *et al*. Mediated imaging and improved targeting of farnesylthiosalicylic acid delivery for pancreatic cancer via conjugation with near-infrared fluorescence heptamethine carbocyanine dye. ACS Appl Bio Mater. 2020; 3: 1129-38.
81. Chen Q, Wang C, Zhan Z, He W, Cheng Z, Li Y, *et al*. Near-infrared dye bound albumin with separated imaging and therapy wavelength channels for imaging-guided photothermal therapy. Biomaterials. 2014; 35: 8206-14.
82. Kalyane D, Raval N, Maheshwari R, Tambe V, Kalia K, Tekade RK. Employment of enhanced permeability and retention effect (EPR): Nanoparticle-based precision tools for targeting of therapeutic and diagnostic agent in cancer. Mater Sci Eng C. 2019; 98: 1252-76.
83. An F, Yang Z, Zheng M, Mei T, Deng G, Guo P, *et al*. Rationally assembled albumin/indocyanine green nanocomplex for enhanced tumor imaging to guide photothermal therapy. J Nanobiotechnology. 2020; 18: 49.
84. An F-F, Zhang X-H. Strategies for preparing albumin-based nanoparticles for multifunctional bioimaging and drug delivery. Theranostics. 2017; 7: 3667.
85. Du B, Qu C, Qian K, Ren Y, Li Y, Cui X, *et al*. An IR820 dye-protein complex for second near-infrared window and photoacoustic imaging. Adv Opt Mater. 2020; 8: 1901471.
86. Thavornpradit S, Usama SM, Lin C-M, Burgess K. Protein labelling and albumin binding characteristics of the near-IR Cy7 fluorophore, QuatCy. Org Biomol Chem. 2019; 17: 7150-4.
87. Tian R, Zeng Q, Zhu S, Lau J, Chandra S, Ertsey R, *et al*. Albumin-chaperoned cyanine dye yields superbright NIR-II fluorophore with enhanced pharmacokinetics. Sci Adv. 2019; 5: eaaw0672.
88. Zhu Y, Huang J, Sun Y, He Z, Feng W, Ren H, *et al*. Tuning Nanoparticle Rigidity: From Megadalton Dendritic Dots to Mechanobiology-Driven Nano-Bio Interactions. ACS nano. 2025; 19: 37339-52.
89. Sun R, Xiang J, Zhou Q, Piao Y, Tang J, Shao S, *et al*. The tumor EPR effect for cancer drug delivery: Current status, limitations, and alternatives. Adv Drug Deliv Rev. 2022; 191: 114614.
90. Sharifi M, Cho WC, Ansariesfahani A, Tarharoudi R, Malekisarvar H, Sari S, *et al*. An updated review on EPR-based solid tumor targeting nanocarriers for cancer treatment. Cancers. 2022; 14: 2868.
91. Champion JA, Katare YK, Mitragotri S. Particle shape: a new design parameter for micro-and nanoscale drug delivery carriers. J Control Release. 2007; 121: 3-9.
92. Cooley M, Sarode A, Hoore M, Fedosov DA, Mitragotri S, Gupta AS. Influence of particle size and shape on their margination and wall-adhesion: implications in drug delivery vehicle design across nano-to-micro scale. Nanoscale. 2018; 10: 15350-64.
93. Irigaray P, Belpomme D. Basic properties and molecular mechanisms of exogenous chemical carcinogens. Carcinogenesis. 2010; 31: 135-48.
94. Devuyst O, Rippe B. Water transport across the peritoneal membrane. Kidney Int. 2014; 85: 750-8.
95. Wu M-R, Huang Y-Y, Hsiao J-K. Use of indocyanine green (ICG), a medical near infrared dye, for enhanced fluorescent imaging-comparison of organic anion transporting polypeptide 1B3 (OATP1B3) and sodium-taurocholate cotransporting polypeptide (NTCP) reporter genes. Molecules. 2019; 24: 2295.
96. Meng X, Yu Z, Xu W, Chai J, Fang S, Min P, *et al*. Control of fibrosis and hypertrophic scar formation via glycolysis regulation with IR780. Burns Trauma. 2022; 10: tkac015.
97. Yang W, Chen Z, Qu L, Zhang C, Chen H, Zheng J, *et al*. IR-780 dye-based targeting of cancer-associated fibroblasts improves cancer immunotherapy by increasing intra-tumoral T lymphocytes infiltration. Curr Cancer Drug Targets. 2024; 24: 642-53.
98. Wang Z, Chen L, Huang Y, Luo M, Wang H, Jiang Z, *et al*. Pharmaceutical targeting of succinate dehydrogenase in fibroblasts controls bleomycin-induced lung fibrosis. Redox Biol. 2021; 46: 102082.
99. Wu JB, Shao C, Li X, Shi C, Li Q, Hu P, *et al*. Near-infrared fluorescence imaging of cancer mediated by tumor hypoxia and HIF1α/OATPs signaling axis. Biomaterials. 2014; 35: 8175-85.
100. Ramachandran A, Betts G, Bhana S, Helme G, Blick C, Moller-Levet C, *et al*. An in vivo hypoxia metagene identifies the novel hypoxia inducible factor target gene SLCO1B3. Eur J Cancer. 2013; 49: 1741-51.
101. Huang Y, Zhou J, Luo S, Wang Y, He J, Luo P, *et al*. Identification of a fluorescent small-molecule enhancer for therapeutic autophagy in colorectal cancer by targeting mitochondrial protein translocase TIM44. Gut. 2018; 67: 307-19.
102. Zhang E, Luo S, Tan X, Shi C. Mechanistic study of IR-780 dye as a potential tumor targeting and drug delivery agent. Biomaterials. 2014; 35: 771-8.
103. Shi C, Wu JB, Chu GC, Li Q, Wang R, Zhang C, *et al*. Heptamethine carbocyanine dye-mediated near-infrared imaging of canine and human cancers through the HIF-1α/OATPs signaling axis. Oncotarget. 2014; 5: 10114.
104. Gao M, Yu F, Lv C, Choo J, Chen L. Fluorescent chemical probes for accurate tumor diagnosis and targeting therapy. Chem Soc Rev. 2017; 46: 2237-71.
105. Duan Z, Zhao J, Sun Y, Wang Z, Piao Y, Shen Y, *et al*. Supramolecular Amino Acids-Encoded Nanodots (SEND) with pH-and Ion-Responsive Phase Separation for Serum-Tolerant Cytosolic Protein Delivery. Adv Mater. 2026; 38: e14041.
106. Han X, Wang R, Song X, Yu F, Lv C, Chen L. A mitochondrial-targeting near-infrared fluorescent probe for bioimaging and evaluating endogenous superoxide anion changes during ischemia/reperfusion injury. Biomaterials. 2018; 156: 134-46.
107. Gogvadze V, Orrenius S, Zhivotovsky B. Mitochondria as targets for chemotherapy. Apoptosis. 2009; 14: 624-40.
108. Zhang E, Zhang C, Su Y, Cheng T, Shi C. Newly developed strategies for multifunctional mitochondria-targeted agents in cancer therapy. Drug Discov Today. 2011; 16: 140-6.
109. Zhang C, Long L, Shi C. Mitochondria-targeting IR-780 dye and its derivatives: synthesis, mechanisms of action, and theranostic applications. Adv Ther. 2018; 1: 1800069.
110. Davis S, Weiss M, Wong J, Lampidis TJ, Chen LB. Mitochondrial and plasma membrane potentials cause unusual accumulation and retention of rhodamine 123 by human breast adenocarcinoma-derived MCF-7 cells. J Biol Chem. 1985; 260: 13844-50.
111. Dietzen DJ, Davis EJ. Excess membrane cholesterol is not responsible for metabolic and bioenergetic changes in AS-30D hepatoma mitochondria. Arch Biochem. 1994; 309: 341-7.
112. Modica-Napolitano JS, Aprille JR. Basis for the selective cytotoxicity of rhodamine 123. Cancer Res. 1987; 47: 4361-5.
113. Zhang C, Wang S, Xiao J, Tan X, Zhu Y, Su Y, *et al*. Sentinel lymph node mapping by a near-infrared fluorescent heptamethine dye. Biomaterials. 2010; 31: 1911-7.
114. Wang Y, Liao X, Sun J, Yi B, Luo S, Liu T, *et al*. Characterization of HIF-1α/Glycolysis Hyperactive Cell Population via Small-Molecule-Based Imaging of Mitochondrial Transporter Activity. Adv Sci. 2018; 5: 1700392.
115. Huang X, Gao M, Xing H, Du Z, Wu Z, Liu J, *et al*. Rationally Designed Heptamethine Cyanine Photosensitizers that Amplify Tumor-Specific Endoplasmic Reticulum Stress and Boost Antitumor Immunity. Small. 2022; 18: 2202728.
116. Deng H, Zhou Z, Yang W, Lin L-s, Wang S, Niu G, *et al*. Endoplasmic reticulum targeting to amplify immunogenic cell death for cancer immunotherapy. Nano Lett. 2020; 20: 1928-33.
117. Mei A, He X, Lei D, Wang L, Wang W, Shao J, *et al*. Squaraine-based NIR dyes for phototheranostics. Coord Chem Rev. 2025; 527: 216419.
118. Park Y, Park MH, Hyun H. Tumor-Targeted Squaraine Dye for near-infrared fluorescence-guided photodynamic therapy. Int J Mol Sci. 2024; 25: 3428.
119. Wan Y, Chen W, Liu Y, Lee KW, Gao Y, Zhang D, *et al*. Neutral cyanine: Ultra-stable NIR-II merocyanines for highly efficient bioimaging and tumor-targeted phototheranostics. Adv Mater. 2024; 36: 2405966.
120. Cai B, Li X, Wang Y, Liu Y, Yang F, Chen H, *et al*. Apoptosis of bone marrow mesenchymal stem cells caused by homocysteine via activating JNK signal. PLoS One. 2013; 8: e63561.
121. Madhavan L. Redox-based regulation of neural stem cell function and Nrf2. Biochem Soc Trans. 2015; 43: 627-31.
122. Zhang C, Liu T, Luo P, Gao L, Liao X, Ma L, *et al*. Near-infrared oxidative phosphorylation inhibitor integrates acute myeloid leukemia-targeted imaging and therapy. Sci Adv. 2021; 7: eabb6104.
123. Wang X, Chen Z, Luo S, Jin T, Wang Y, Chen F, *et al*. Development of Therapeutic Small-Molecule Fluorophore for Cell Transplantation. Adv Funct Mater. 2016; 26: 8397-407.
124. Zhao Y, Kong C, Chen X, Wang Z, Wan Z, Jia L, *et al*. Repetitive exposure to low-dose X-irradiation attenuates testicular apoptosis in type 2 diabetic rats, likely via Akt-mediated Nrf2 activation. Mol Cell Endocrinol. 2016; 422: 203-10.
125. Wang J, Dai L, Yue X, Shen C, Li T, Long L, *et al*. IR-61 improves voiding function via mitochondrial protection in diabetic rats. Front Pharmacol. 2021; 12: 608637.
126. Yue X-F, Shen C-X, Wang J-W, Dai L-Y, Fang Q, Long L, *et al*. The near-infrared dye IR-61 restores erectile function in a streptozotocin-induced diabetes modelvia mitochondrial protection. Asian J Androl. 2021; 23: 249-58.
127. Wang Y, Tang B, Li H, Zheng J, Zhang C, Yang Z, *et al*. A small-molecule inhibitor of Keap1–Nrf2 interaction attenuates sepsis by selectively augmenting the antibacterial defence of macrophages at infection sites. EBioMedicine. 2023; 90:104480.
128. Li J, Shen C, Qiu H, Wang J, Yue X, Dai L, *et al*. Intravesical IR-780 instillation prevents radiation cystitis by protecting urothelial integrity. Neurourol Urodyn. 2023; 42: 40-8.
129. Zhang C, Zheng J, Chen W, Yang W, Tan X, Fan X, *et al*. Mitochondrial-targeting fluorescent small molecule IR-780 alleviates radiation-induced brain injury. Brain Res. 2023; 1805: 148285.
130. Finnerty CC, Jeschke MG, Branski LK, Barret JP, Dziewulski P, Herndon DN. Hypertrophic scarring: the greatest unmet challenge after burn injury. Lancet. 2016; 388: 1427-36.

131. Gurtner GC, Werner S, Barrandon Y, Longaker MT. Wound repair and regeneration. Nature. 2008; 453: 314-21.
132. Kalluri R. The biology and function of fibroblasts in cancer. Nat Rev Cancer 2016; 16: 582-98.
133. Xie N, Tan Z, Banerjee S, Cui H, Ge J, Liu R-M, *et al*. Glycolytic reprogramming in myofibroblast differentiation and lung fibrosis. Am J Respir Crit Care Med. 2015; 192: 1462-74.
134. Zhang H, Wang D, Li M, Plecitá-Hlavatá L, D'Alessandro A, Tauber J, *et al*. Metabolic and proliferative state of vascular adventitial fibroblasts in pulmonary hypertension is regulated through a microRNA-124/PTBP1 (polypyrimidine tract binding protein 1)/pyruvate kinase muscle axis. Circulation. 2017; 136: 2468-85.
135. Zhao X, Psarianos P, Ghoraie LS, Yip K, Goldstein D, Gilbert R, *et al*. Metabolic regulation of dermal fibroblasts contributes to skin extracellular matrix homeostasis and fibrosis. Nat Metab. 2019; 1: 147-57.
136. Choi S-H, Hong Z-Y, Nam J-K, Lee H-J, Jang J, Yoo RJ, *et al*. A hypoxia-induced vascular endothelial-to-mesenchymal transition in development of radiation-induced pulmonary fibrosis. Clinical Cancer Research. 2015; 21: 3716-26.
137. Kalluri R, Weinberg RA. The basics of epithelial-mesenchymal transition. J Clin Invest. 2009; 119: 1420-8.
138. Ranchoux B, Antigny F, Rucker-Martin C, Hautefort A, Péchoux C, Bogaard HJ, *et al*. Endothelial-to-mesenchymal transition in pulmonary hypertension. Circulation. 2015; 131: 1006-18.
139. Gibbons MA, MacKinnon AC, Ramachandran P, Dhaliwal K, Duffin R, Phythian-Adams AT, *et al*. Ly6C^{hi} monocytes direct alternatively activated profibrotic macrophage regulation of lung fibrosis. Am J Respir Crit Care Med. 2011; 184: 569-81.
140. Redente EF, Keith RC, Janssen W, Henson PM, Ortiz LA, Downey GP, *et al*. Tumor necrosis factor-α accelerates the resolution of established pulmonary fibrosis in mice by targeting profibrotic lung macrophages. Am J Respir Cell Mol Biol. 2014; 50: 825-37.
141. Vernon MA, Mylonas KJ, Hughes J. Macrophages and renal fibrosis. Semin Nephrol. 2010; 30: 302-17.
142. Luo M, Chen L, Zheng J, Wang Q, Huang Y, Liao F, *et al*. Mitigation of radiation-induced pulmonary fibrosis by small-molecule dye IR-780. Free Radic Biol Med. 2021; 164: 417-28.
143. Berman B, Maderal A, Raphael B. Keloids and hypertrophic scars: pathophysiology, classification, and treatment. Dermatol Surg. 2017; 43: S3-S18.
144. Lee HJ, Jang YJ. Recent understandings of biology, prophylaxis and treatment strategies for hypertrophic scars and keloids. Int J Mol Cell Med. 2018; 19: 711.
145. Ding H, Jiang L, Xu J, Bai F, Zhou Y, Yuan Q, *et al*. Inhibiting aerobic glycolysis suppresses renal interstitial fibroblast activation and renal fibrosis. Am J Physiol Renal Physiol. 2017; 313: F561-F75.
146. Acerbi I, Cassereau L, Dean I, Shi Q, Au A, Park C, *et al*. Human breast cancer invasion and aggression correlates with ECM stiffening and immune cell infiltration. Integr Biol. 2015; 7: 1120-34.
147. Berdiel-Acer M, Sanz-Pamplona R, Calon A, Cuadras D, Berenguer A, Sanjuan X, *et al*. Differences between CAFs and their paired NCF from adjacent colonic mucosa reveal functional heterogeneity of CAFs, providing prognostic information. Mol Oncol. 2014; 8: 1290-305.
148. Chaudhuri O, Koshy ST, Branco da Cunha C, Shin J-W, Verbeke CS, Allison KH, *et al*. Extracellular matrix stiffness and composition jointly regulate the induction of malignant phenotypes in mammary epithelium. Nat Mater. 2014; 13: 970-8.
149. Liang Y, Zhou X, Liu W, Shang L. Multichannel Sensor Arrays Based on Surface-Engineered Fluorescent Metal Clusterzymes for Differential Sensing of Cancer Cells. J Anal Test. 2025; 9: 183-92.
150. Suo Y, Liu T, Xie C, Wei D, Tan X, Wu L, *et al*. Near infrared in vivo flow cytometry for tracking fluorescent circulating cells. Cytometry A. 2015; 87: 878-84.
151. Alzubaidi FM, Liu Q, Manzhos S, Sonar P, Izake EL, Ayoko GA. A New Disposable Paper-Based Chemosensor for the Rapid and Direct Detection of Hexavalent Chromium in Aqueous Media. J Anal Test. 2025; 9: 607-617.
152. Li X, Yang Y, Zhang R, Huang W. Construction and optimization of organic fluorophores in NIR-II fluorescence imaging. Chem Soc Rev. 2025; 54: 11184-11225.
153. Li X, Zhang R, Yang Y, Huang W. Finely tailored conjugated small molecular nanoparticles for near-infrared biomedical applications. Research. 2025; 8: 0534.
154. Luo S, Yang X, Shi C. Newly emerging theranostic agents for simultaneous cancertargeted imaging and therapy. Curr Med Chem. 2016; 23: 483-97.
155. Luo S, Zhang E, Su Y, Cheng T, Shi C. A review of NIR dyes in cancer targeting and imaging. Biomaterials. 2011; 32: 7127-38.
156. Shi C, Zhang C, Su Y, Cheng T. Cyanine dyes in optical imaging of tumours. Lancet Oncol. 2010; 11: 815-6.
157. Ishizawa T, Masuda K, Urano Y, Kawaguchi Y, Satou S, Kaneko J, *et al*. Mechanistic background and clinical applications of indocyanine green fluorescence imaging of hepatocellular carcinoma. Ann Surg Oncol. 2014; 21: 440-8.
158. Shibasaki Y, Sakaguchi T, Hiraide T, Morita Y, Suzuki A, Baba S, *et al*. Expression of indocyanine green-related transporters in hepatocellular carcinoma. J Surg Res. 2015; 193: 567-76.
159. Park Y, Park MH, Hyun H. Structure-inherent tumor-targeted IR-783 for near-infrared fluorescence-guided photothermal therapy. Int J Mol Sci. 2024; 25: 5309.
160. Ren H, Zeng X-Z, Zhao X-X, Hou D-Y, Yao H, Yaseen M, *et al*. A bioactivated in vivo assembly nanotechnology fabricated NIR probe for small pancreatic tumor intraoperative imaging. Nat Commun. 2022; 13: 418.
161. Ding Q, Wang X, Luo Y, Leng X, Li X, Gu M, *et al*. Mitochondria-targeted fluorophore: State of the art and future trends. Coord Chem Rev. 2024; 508: 215772.
162. Wang Y, Liu T, Zhang E, Luo S, Tan X, Shi C. Preferential accumulation of the near infrared heptamethine dye IR-780 in the mitochondria of drug-resistant lung cancer cells. Biomaterials. 2014; 35: 4116-24.
163. Luo P, Tan X, Luo S, Wang Z, Long L, Wang Y, *et al*. An NIR-Fluorophore-Based Inhibitor of SOD1 Induces Apoptosis by Targeting Transcription Cofactor PC4. Adv Ther. 2019; 2: 1800148.
164. Shen C, Yue X, Dai L, Wang J, Li J, Fang Q, *et al*. Hyperbaric Oxygen Enhanced Mitochondria-Targeted Chemotherapy in Bladder Cancer. J Cancer Res Clin Oncol. 2023; 149: 683-699.
165. Vyas S, Zaganjor E, Haigis MC. Mitochondria and cancer. Cell. 2016; 166: 555-66.
166. Jiang Q, Zhang C, Wang H, Peng T, Zhang L, Wang Y, *et al*. Mitochondria-targeting immunogenic cell death inducer improves the adoptive T-cell therapy against solid tumor. Front Oncol. 2019; 9: 1196.
167. Lee JJ, Beumer JH, Chu E. Therapeutic drug monitoring of 5-fluorouracil. Cancer Chemother Pharmacol. 2016; 78: 447-64.
168. Tian Y, Younis MR, Tang Y, Liao X, He G, Wang S, *et al*. Dye-loaded mesoporous polydopamine nanoparticles for multimodal tumor theranostics with enhanced immunogenic cell death. J Nanobiotechnology. 2021; 19: 365.
169. Qin Y, Wang G, Chen L, Sun Y, Yang J, Piao Y, *et al*. High-throughput screening of surface engineered cyanine nanodots for active transport of therapeutic antibodies into solid tumor. Adv Mater. 2024; 36: 2302292.
170. Yue L, He L, Liu N, Pan R, Zhu J. Synthesis and Cancer Biomedical Applications of Dendrimer-Based Fluorescence Imaging Agents. Prog Chem. 2024; 36: 1186-99.
171. Surekha B, Kommana NS, Dubey SK, Kumar AP, Shukla R, Kesharwani P. PAMAM dendrimer as a talented multifunctional biomimetic nanocarrier for cancer diagnosis and therapy. Colloids Surf B Biointerfaces. 2021; 204: 111837.
172. Huang T, Li G, Guo Y, Zhang G, Shchabin D, Shi X, *et al*. Recent advances in PAMAM dendrimer-based CT contrast agents for molecular imaging and theranostics of cancer. Sens Diagn. 2023; 2: 1145-57.
173. Kim Y, Kim SH, Tanyeri M, Katzenellenbogen JA, Schroeder CM. Dendrimer probes for enhanced photostability and localization in fluorescence imaging. Biophys J. 2013; 104: 1566-75.
174. Abbasi E, Aval SF, Akbarzadeh A, Milani M, Nasrabadi HT, Joo SW, *et al*. Dendrimers: synthesis, applications, and properties. Nanoscale Res Lett. 2014; 9: 247.
175. Ji C, Cheng W, Yuan Q, Mullen K, Yin M. From dyestuff chemistry to cancer theranostics: the rise of rylenecarboximides. Acc Chem Res. 2019; 52: 2266-77.
176. Zhu Y, Fang Y, Huang W, Zhang W, Chen F, Dong J, *et al*. AI-driven precision subcellular navigation with fluorescent probes. J Mater Chem B. 2024; 12: 11054-62.
177. Kobayashi H, Choyke PL. Target-cancer-cell-specific activatable fluorescence imaging probes: rational design and in vivo applications. Acc Chem Res. 2011; 44: 83-90.
178. Mochida A, Ogata F, Nagaya T, Choyke PL, Kobayashi H. Activatable fluorescent probes in fluorescence-guided surgery: Practical considerations. Bioorg Med Chem. 2018; 26: 925-30.
179. Wu M, Gong D, Zhou Y, Zha Z, Xia X. Activatable probes with potential for intraoperative tumor-specific fluorescence-imaging guided surgery. J Mater Chem B. 2023; 11: 9777-97.
180. James NS, Cheruku RR, Missert JR, Sunar U, Pandey RK. Measurement of cyanine dye photobleaching in photosensitizer cyanine dye conjugates could help in optimizing light dosimetry for improved photodynamic therapy of cancer. Molecules. 2018; 23: 1842.
181. Gorka AP, Schnermann MJ. Harnessing cyanine photooxidation: from slowing photobleaching to near-IR uncaging. Curr Opin Chem Biol. 2016; 33: 117-25.
182. Feng L, Chen W, Ma X, Liu SH, Yin J. Near-infrared heptamethine cyanines (Cy7): from structure, property to application. Org Biomol Chem. 2020; 18: 9385-97.
183. Wang T, Li S, Zou Z, Hai L, Yang X, Jia X, *et al*. A zeolitic imidazolate framework-8-based indocyanine green theranostic agent for infrared fluorescence imaging and photothermal therapy. J Mater Chem B. 2018; 6: 3914-21.
184. Xia W-L, Ran X-Y, Xie K-P, Zhao Y, Chen J, Zhou Q, *et al*. Optimized indocyanine green nanopreparations for biomedical applications. Coord Chem Rev. 2025; 528: 216422.
185. Feng E, Jiao L, Tang S, Chen M, Lv S, Liu D, *et al*. Anti-photobleaching cyanine-based nanoparticles with simultaneous PET and ACQ effects for improved tumor photothermal therapy. Chem Eng J. 2022; 432: 134355.
186. Qi Q, Li J, Qiao Q, Yan C, Izadyar M, Wang C, *et al*. Oxazolidine-Caged Heptamethine Cyanine Switch Exhibits High Photostability for Bioimaging via Buffering Fluorogenicity. CCS Chem. 2025; 7: 3409-20.
187. Yin K, Yu F, Liu D, Xie Z, Chen L. Cyanine-based colorimetric and fluorescent probe for the selective detection of diethylstilbestrol in seawater, shrimp and fish samples. Sens Actuators B Chem. 2016; 223: 799-805.

188. Liu S, Dong W, Gao H-q, Song Z, Cheng Z. Near-Infrared-II Fluorescent Probes for Analytical Applications: From In Vitro Detection to In Vivo Imaging Monitoring. Acc Chem Res. 2025; 58: 543-54.
189. Qu S, Xu R, Yi G, Li Z, Zhang H, Qi S, *et al*. Patient-derived organoids in human cancer: a platform for fundamental research and precision medicine. Mol Biomed. 2024; 5: 6.
190. Wu X, Fan Y, Wang K, Miao Y, Chang Y, Ming J, *et al*. NIR-II imaging-guided precise photodynamic therapy for augmenting tumor-starvation therapy by glucose metabolism reprogramming interference. Sci Bull. 2024; 69: 1263-74.
191. Zhu J, Jiang Y, Pan X, Xu K, Niu W, Lv Y, *et al*. In Vivo Evaluation of a Gallium-68-Labeled Tumor-Tracking Cyanine Dye for Positron Emission Tomography/Near-Infrared Fluorescence Carcinoma Imaging, Image-Guided Surgery, and Photothermal Therapy. ACS omega. 2023; 8: 6067-77.
192. Li X, Schumann C, Albarqi HA, Lee CJ, Alani AW, Bracha S, *et al*. A tumor-activatable theranostic nanomedicine platform for NIR fluorescence-guided surgery and combinatorial phototherapy. Theranostics. 2018; 8: 767.
193. Liu Y, Diao S, Ruan B, Zhou Y, Yu M, Dong G, *et al*. Molecular engineering of activatable NIR-II hemicyanine reporters for early diagnosis and prognostic assessment of inflammatory bowel disease. ACS nano. 2024; 18: 8437-51.
194. Verma N, Setia A, Mehata AK, Randhave N, Badgujar P, Malik AK, *et al*. Recent advancement of indocyanine green based nanotheranostics for imaging and therapy of coronary atherosclerosis. Mol Pharm. 2024; 21: 4804-26.